LPT-07-11
CPHT-RR002.0107
hep-ph/0703166

Diffractive production of two ρ_L^0 mesons in e^+e^- collisions

M. Segond,[a] L. Szymanowski[a,b,c,d] and S. Wallon[a]

[a] LPT, Université Paris-Sud -CNRS, 91405-Orsay, France

[b] Soltan Institute for Nuclear Studies, Warsaw, Poland

[c] Université de Liège, B4000 Liège, Belgium

[d] CPHT, École Polytechnique-CNRS, 91128 Palaiseau, France

Abstract

We present an estimate of the cross-section for the exclusive production of a ρ_L^0-meson pair in e^+e^- scattering, which will be studied in the future high energy International Linear Collider. For this aim, we complete calculations of the Born order approximation of the amplitudes $\gamma^*_{L,T}(Q_1^2)\gamma^*_{L,T}(Q_2^2) \to \rho_L^0\rho_L^0$, for arbitrary polarization of virtual photons and longitudinally polarized mesons, in the kinematical region $s \gg -t$, $Q_1^2\,, Q_2^2$. These processes are completely calculable in the hard region $Q_1^2\,, Q_2^2 \gg \Lambda^2_{QCD}$ and we perform most of the calculations in an analytical way. The resulting cross-section turns out to be large enough for this process to be measurable with foreseen luminosity and energy, for Q_1^2 and Q_2^2 in the range of a few GeV^2.

1 Introduction

The next generation of e^+e^--colliders will offer a possibility of clean testing of QCD dynamics. By selecting events in which two vector mesons are produced with large rapidity gap, through scattering of two highly virtual photons, one is getting access to the kinematical regime in which the perturbative approach is justified. If additionally one selects the events with comparable photon virtualities, the perturbative Regge dynamics of QCD of the BFKL [1] type should dominate with respect to the conventional partonic evolution of DGLAP [2] type. Several studies of BFKL dynamics have been performed at the level of the total cross-section [3, 4].

In the paper [5] the diffractive production of two J/Ψ mesons was studied as a promising probe of the BFKL effects. Recently, we have advocated [6, 7, 8] that the electroproduction of two $\rho-$mesons in the $\gamma^*\gamma^*$ offers the same advantages. In this case the virtualities of the scattered photons play the role of the hard scales. A first step in this direction was made by considering this process with longitudinally polarized photons and $\rho-$mesons,

$$\gamma_L^*(q_1)\,\gamma_L^*(q_2) \to \rho_L^0(k_1)\,\rho_L^0(k_2)\,, \tag{1.1}$$

for arbitrary values of $t = (q_1 - k_1)^2$, with $s \gg -t$. The choice of longitudinal polarizations of both the scattered photons and produced vector mesons was dictated by the fact that this configuration of the lowest twist-2 gives the dominant contribution in the powers of the hard scale Q^2, when $Q_1^2 \sim Q_2^2 \sim Q^2$.

The aim of this study is to complete the Born order evaluation of the cross-section of the process

$$e^+e^- \to e^+e^-\rho_L^0\rho_L^0\,, \tag{1.2}$$

illustrated in Fig.1. We calculated contributions with remaining combinations of polar-

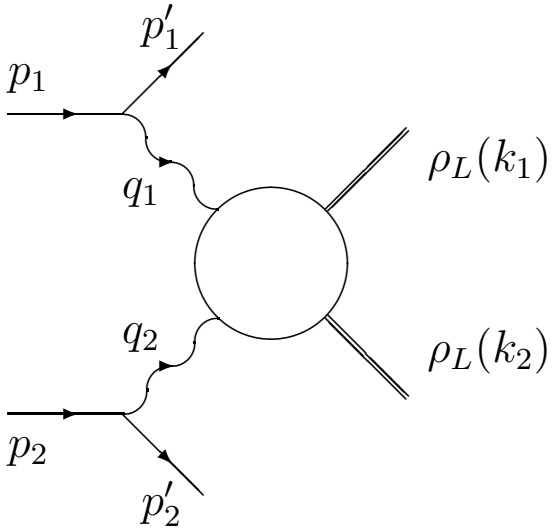

Figure 1: Amplitude for the process $e^+\,e^- \to e^+\,e^-\,\rho_L^0\,\rho_L^0$.

izations of virtual photons necessary to obtain all helicity amplitudes of the processes

$$\gamma^*_{L,T}(q_1)\,\gamma^*_{L,T}(q_2) \to \rho^0_L(k_1)\,\rho^0_L(k_2)\,. \tag{1.3}$$

Let us note, that the double tagging of final leptons gives in particular the possibility to separate the contributions of various photon polarizations, entering in (1.2) and thus to study the corresponding parts of the cross-sections which are computed in this paper. We are focusing here on the high-energy limit in which $t-$channel gluonic exchanges dominate. On the other hand, in the description of the process (1.2), there is a potential possibility that also contributions with rather small $s_{\gamma^*\gamma^*}$ have to be taken into account. In this case one should include in principle both quark and gluon exchanges. The contribution of quark exchange was analyzed in [9]. This quark-box contribution is investigated in subsection 4.3.

We will also not consider here the case of transversally polarized $\rho-$mesons. It would require to deal with possible breaking of QCD factorization [10], although a method to overcome this problem has been proposed [11].

The BFKL enhancement was studied for $t = 0$ in [8] and [12]. In this latter case, the peculiar value $t = 0$ automatically selects the longitudinally polarized photon. A dedicate study for arbitrary value of t should thus be performed to get an evaluation of BFKL enhancement effects of the Born order evaluation performed in the present paper for transversally polarized photon. This problem will not be addressed here.

2 Kinematics

The measurable cross section for the process (1.2) of Fig.1 is related to the amplitude of the process (1.3), illustrated in Fig.2, through the usual flux factors for respectively transversally and longitudinally polarized photons

$$t(y_i) = \frac{1+(1-y_i)^2}{2}, \quad l(y_i) = 1-y_i\,, \tag{2.1}$$

where y_i $(i = 1, 2)$ are the longitudinal momentum fractions of the bremsstrahlung photons with respect to the incoming leptons. This relation reads [13]

$$\begin{aligned}
&\frac{d\sigma(e^+e^- \to e^+e^-\rho^0_L\rho^0_L)}{dy_1 dy_2 dQ_1^2 dQ_2^2} \\
&= \frac{1}{y_1 y_2\, Q_1^2 Q_2^2}\left(\frac{\alpha}{\pi}\right)^2 \left[l(y_1)\,l(y_2)\,\sigma(\gamma^*_L\gamma^*_L \to \rho^0_L\rho^0_L) + \; t(y_1)\,l(y_2)\,\sigma(\gamma^*_T\gamma^*_L \to \rho^0_L\rho^0_L)\right. \\
&\left. +\; l(y_1)\,t(y_2)\,\sigma(\gamma^*_L\gamma^*_T \to \rho^0_L\rho^0_L) + t(y_1)\,t(y_2)\,\sigma(\gamma^*_T\gamma^*_T \to \rho^0_L\rho^0_L)\right]\,.
\end{aligned} \tag{2.2}$$

The presence of hard scales Q_i^2 permits us to apply the collinear approximation at each $q\bar{q}\rho-$meson vertex, and the use of distribution amplitude (DA) for describing the $q\bar{q}$ content of the ρ mesons, as illustrated in Fig.2. In this paper, except for section 4.3, the amplitude M_H will be described using the impact representation, valid at high energy, as illustrated in Fig.3.

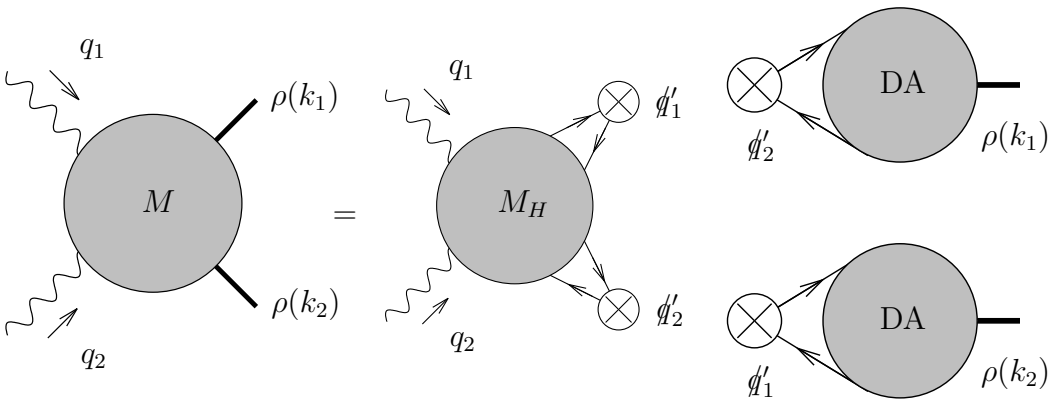

Figure 2: The amplitude of the process $\gamma^*(Q_1)\gamma^*(Q_2) \to \rho_L^0(k_1)\rho_L^0(k_2)$ with the collinear factorization in the $q\bar{q}\rho$ vertex.

Let us introduce two light-like Sudakov vectors q_1' and q_2' which form a natural basis for two scattered virtual photons, which satisfy $2q_1' \cdot q_2' \equiv s \sim 2q_1 \cdot q_2$. The usual $s_{\gamma^*\gamma^*}$ is related to the auxiliary useful variable s by $s_{\gamma^*\gamma^*} = s - Q_1^2 - Q_2^2$. The momentum transfer in the $t-$channel is $r = k_1 - q_1$. In this basis, the incoming photon momenta read

$$q_1 = q_1' - \frac{Q_1^2}{s} q_2' \quad \text{and} \quad q_2 = q_2' - \frac{Q_2^2}{s} q_1' \,. \tag{2.3}$$

The polarization vectors of longitudinally polarized photons are

$$\epsilon_\mu^{L(1)} = \frac{q_{1\mu}}{Q_1} + \frac{2Q_1}{s} q_{2\mu}' \quad \text{and} \quad \epsilon_\mu^{L(2)} = \frac{q_{2\mu}}{Q_2} + \frac{2Q_2}{s} q_{1\mu}' \,, \tag{2.4}$$

with $\epsilon_{L(i)}^2 = 1$ and $q_i \cdot \epsilon_{L(i)} = 0$, whereas the polarization vectors of transversally polarized photons are two dimensional transverse vectors satisfying $\epsilon_{T(i)}^2 = -1$ $(i = 1, 2)$ and $q_i \cdot \epsilon_{T(i)} = 0$.

We label the momentum of the quarks and antiquarks entering the meson wave functions as l_1 and l_1' for the upper part of the diagram and l_2 and l_2' for the lower part (see Fig.3).

In the basis (2.3), the vector meson momenta can be expanded in the form

$$\begin{aligned} k_1 &= \alpha(k_1)\, q_1' + \frac{\underline{r}^2}{\alpha(k_1)\, s} q_2' + r_\perp \,, \\ k_2 &= \beta(k_2)\, q_2' + \frac{\underline{r}^2}{\beta(k_2)\, s} q_1' - r_\perp \,. \end{aligned} \tag{2.5}$$

Note that our convention is such that for any tranverse vector $v_\perp$ in Minkowski space, $\underline{v}$ denotes its euclidean form. In the following, we will treat the ρ meson as being massless. α and β are very close to unity (explicit expressions can be found in [7]), and reads

$$\begin{aligned} \alpha(k_1) &\simeq 1 - \frac{Q_2^2 + \underline{r}^2}{s} + O\left(\frac{1}{s^2}\right) \,, \\ \beta(k_2) &\simeq 1 - \frac{Q_1^2 + \underline{r}^2}{s} + O\left(\frac{1}{s^2}\right) \,, \end{aligned} \tag{2.6}$$

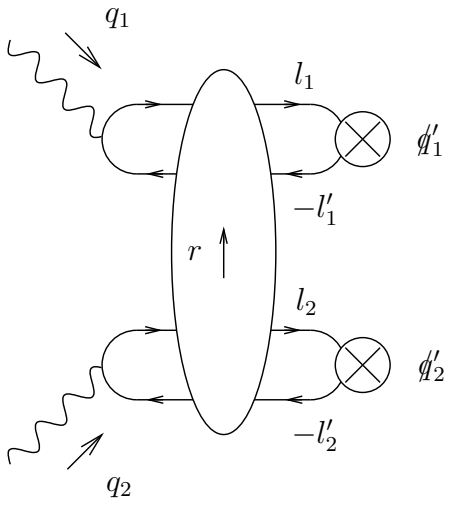

Figure 3: The amplitude M_H in the impact representation. The vertical blob symbolizes the interaction of two $q\bar{q}$ dipoles through gluon exchanges at high s.

where $\underline{r}^2 = -r_\perp^2$. They will be replaced by 1 in the phenomenological applications of sections 4 and 5. In this decomposition, it is straightforward to relate $t = r^2$ to $\underline{r}^2$ through the approximate relation

$$t \sim -\frac{Q_1^2\, Q_2^2}{s} - \underline{r}^2 \left(1 + \frac{Q_1^2}{s} + \frac{Q_2^2}{s} + \frac{\underline{r}^2}{s}\right) \tag{2.7}$$

(see [7] for an exact relation). From Eq.(2.7) the threshold for $|t|$ is given by $|t|_{min} = Q_1^2 Q_2^2/s$, corresponding to $r_\perp = 0$. In the kinematical range we are interested in, the relation (2.7) can be approximated as $\underline{r}^2 = -t$, as usually in the Regge limit.

The links with the e^+e^- process can be made by using the same Sudakov basis for the two incoming leptons:

$$p_1 = \frac{1}{y_1} q'_1 + y_1 \frac{\underline{p}_1^2}{s} q'_2 + p_{\perp 1} \quad \text{and} \quad p_2 = \frac{1}{y_2} q'_2 + y_2 \frac{\underline{p}_2^2}{s} q'_1 + p_{\perp 2}\,, \quad \text{with} \quad \underline{p}_i^2 = \frac{1-y_i}{y_i^2} Q_i^2\,. \tag{2.8}$$

Thus, one gets

$$s_{e^+e^-} = \frac{s}{y_1 y_2} \left(1 + \frac{(1-y_1)(1-y_2) Q_1^2 Q_2^2}{s^2}\right) - 2\underline{p}_1 \cdot \underline{p}_2\,.$$

In the rest of the paper, since we keep only the dominant s contribution, we use the approximate relation $s_{e^+e^-} \sim s/(y_1 y_2)$.

3 Impact representation

The impact factor representation of the scattering amplitude for the process (1.3) has the form (see Fig.4)

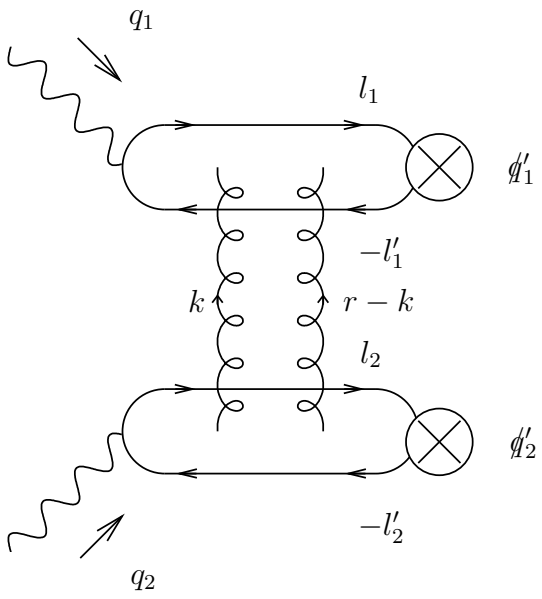

Figure 4: Amplitude M_H at Born order. The t-channel gluons are attached to the quark lines in all possible ways.

$$\mathcal{M} = is \int \frac{d^2\,\underline{k}}{(2\pi)^4 \underline{k}^2\,(\underline{r}-\underline{k})^2} \mathcal{J}^{\gamma^*_{L,T}(q_1)\to\rho^0_L(k_1)}(\underline{k},\underline{r}-\underline{k})\;\mathcal{J}^{\gamma^*_{L,T}(q_2)\to\rho^0_L(k_2)}(-\underline{k},-\underline{r}+\underline{k})\,, \quad (3.1)$$

where $\mathcal{J}^{\gamma^*_{L,T}(q_1)\to\rho^0_L(k_1)}(\underline{k},\underline{r}-\underline{k})$ ($\mathcal{J}^{\gamma^*_{L,T}(q_2)\to\rho^0_L(k_2)}(\underline{k},\underline{r}-\underline{k})$) are the impact factors corresponding to the transition of $\gamma^*_{L,T}(q_1) \to \rho^0_L(k_1)$ ($\gamma^*_{L,T}(q_2) \to \rho^0_L(k_2)$) via the $t-$channel exchange of two gluons. The amplitude (3.1) calculated in Born order depends linearly on s (or $s_{\gamma^*\gamma^*}$ when neglecting terms of order Q_i^2/s) as the impact factors are s-independent.

Calculations of the impact factors in the Born approximation[1]are standard [14]. They are obtained by assuming the collinear approximation at each $q\bar{q}\rho-$meson vertex. Projecting the (anti)quark momenta on the Sudakov basis q_1', q_2',

$$\begin{aligned}
l_1 &= z_1 q_1' + l_{\perp 1} + z_1 r_\perp - \frac{(l_{\perp 1} + z_1 r_\perp)^2}{z_1 s} q_2' \,, \\
l_1' &= \bar{z}_1 q_1' - l_{\perp 1} + \bar{z}_1 r_\perp - \frac{(-l_{\perp 1} + \bar{z}_1 r_\perp)^2}{\bar{z}_1 s} q_2' \,, \\
l_2 &= z_2 q_2' + l_{\perp 2} - z_2 r_\perp - \frac{(l_{\perp 2} - z_2 r_\perp)^2}{z_2 s} q_1' \,, \\
l_2' &= \bar{z}_2 q_2' - l_{\perp 2} - \bar{z}_2 r_\perp - \frac{(-l_{\perp 2} - \bar{z}_2 r_\perp)^2}{\bar{z}_2 s} q_1' \,,
\end{aligned} \quad (3.2)$$

we put the relative momentum $l_{i\perp}$ to zero. For longitudinally polarized photons the

[1]Now, the forward impact factor of $\gamma^*_L(Q^2) \to \rho^0_L$ transition has been calculated at the next-to-leading order accuracy in [15].

impact factor reads

$$\mathcal{J}^{\gamma_L^*(q_i)\to\rho_L(k_i)}(\underline{k},\underline{r}-\underline{k}) = 8\pi^2\alpha_s\frac{e}{\sqrt{2}}\frac{\delta^{ab}}{2N_c}Q_i\, f_\rho\, \alpha(k_i)\int\limits_0^1 dz_i z_i\, \bar{z}_i\, \phi(z_i)\mathrm{P_P}(\mathrm{z_i},\underline{\mathrm{k}},\underline{\mathrm{r}},\mu_\mathrm{i})\,, \tag{3.3}$$

where the expression

$$\mathrm{P_P}(\mathrm{z_i},\underline{\mathrm{k}},\underline{\mathrm{r}},\mu_\mathrm{i}) = \frac{1}{\mathrm{z_i^2}\underline{\mathrm{r}}^2+\mu_\mathrm{i}^2} + \frac{1}{\bar{\mathrm{z}}_\mathrm{i}^2\underline{\mathrm{r}}^2+\mu_\mathrm{i}^2} - \frac{1}{(\mathrm{z_i}\underline{\mathrm{r}}-\underline{\mathrm{k}})^2+\mu_\mathrm{i}^2} - \frac{1}{(\bar{\mathrm{z}}_\mathrm{i}\underline{\mathrm{r}}-\underline{\mathrm{k}})^2+\mu_\mathrm{i}^2} \tag{3.4}$$

originates from the impact factor of quark pair production from a longitudinally polarized photon.

For transversally polarized photons, one obtains

$$\begin{aligned}&\mathcal{J}^{\gamma_T^*(q_i)\to\rho_L(k_i)}(\underline{k},\underline{r}-\underline{k})\\ &= 4\pi^2\alpha_s\frac{e}{\sqrt{2}}\frac{\delta^{ab}}{2N_c}\, f_\rho\alpha(k_i)\int\limits_0^1 dz_i\,(z_i-\bar{z}_i)\,\phi(z_i)\,\underline{\epsilon}\cdot\underline{\mathrm{Q}}(z_i,\underline{k},\underline{r},\mu_i)\,,\end{aligned} \tag{3.5}$$

where

$$\underline{Q}(z_i,\underline{k},\underline{r},\mu_i) = \frac{z_i\,\underline{r}}{z_i^2\underline{r}^2+\mu_i^2} - \frac{\bar{z}_i\,\underline{r}}{\bar{z}_i^2\underline{r}^2+\mu_i^2} + \frac{\underline{k}-z_i\,\underline{r}}{(z_i\underline{r}-\underline{k})^2+\mu_i^2} - \frac{\underline{k}-\bar{z}_i\underline{r}}{(\bar{z}_i\,\underline{r}-\underline{k})^2+\mu_i^2} \tag{3.6}$$

is proportional to the impact factor of quark pair production from a transversally polarized photon.

In the formulae (3.4) and (3.6) and for the rest of the paper, we denote $\mu_i^2 = Q_i^2\; z_i\; \bar{z}_i + m^2$, where m is the quark mass. The limit $m \to 0$ is regular and we will restrict ourselves to the light quark case, taking thus $m = 0$. Both impact factor (3.4) and (3.6) vanish when $\underline{k} \to 0$ or $\underline{r}-\underline{k} \to 0$ due to QCD gauge invariance.

In the formulae (3.3, 3.5), ϕ is the distribution amplitude of the produced longitudinally polarized ρ^0-mesons. For the case with quark q of one flavour it is defined (see, e.g. [16]) by the matrix element of the non-local, gauge invariant correlator of quark fields on the light-cone

$$\langle 0|\bar{q}(x)\;\gamma^\mu\; q(-x)|\rho_L(p) = \bar{q}q\rangle = f_\rho\; p^\mu\int\limits_0^1 dz\, e^{i(2z-1)(px)}\phi(z)\;, \tag{3.7}$$

where the coupling constant is $f_\rho = 216$ MeV and where the gauge links are omitted to simplify the notation. ϕ is normalized to unity. The amplitudes for production of ρ^0's are obtained by noting that $|\rho^0\rangle = 1/\sqrt{2}(|\bar{u}u\rangle - |\bar{d}d\rangle)$.

We label the amplitudes for the scattering process (1.3) through the polarization of the incoming virtual photons as $\mathcal{M}_{\lambda_1\lambda_2}$. They can be calculated using Eqs.(3.1) and Eqs.(3.3-3.6) supplemented by the choice of the transverse polarization vectors of the photons

$$\underline{\epsilon}^{\pm} = \frac{1}{\sqrt{2}}(\mp 1, -i) \tag{3.8}$$

and the longitudinal polarization vectors (2.4). For the case $\lambda_1 = \lambda_2 = 0$:

$$\mathcal{M}_{00} = i\, s\, C\, Q_1\, Q_2 \int_0^1 dz_1\, dz_2\, z_1\, \bar{z}_1\, \phi(z_1)\, z_2\, \bar{z}_2\, \phi(z_2) \mathrm{M}_{00}(z_1,\, z_2)\,, \tag{3.9}$$

with

$$\mathrm{M}_{00}(z_1,\, z_2) = \int \frac{d^2\underline{k}}{\underline{k}^2 (\underline{r} - \underline{k})^2}\, \mathrm{P_P}(\mathrm{z}_1, \underline{\mathrm{k}}, \underline{\mathrm{r}}, \mu_1)\, \mathrm{P_P}(\mathrm{z}_2, -\underline{\mathrm{k}}, -\underline{\mathrm{r}}, \mu_2)\,; \tag{3.10}$$

for the case $\lambda_2 = +, -$:

$$\mathcal{M}_{0\lambda_2} = i\, s\, \frac{C}{2}\, Q_1 \int_0^1 dz_1\, dz_2\, z_1\, \bar{z}_1\, \phi(z_1)\, (z_2 - \bar{z}_2)\, \phi(z_2) \mathrm{M}_{0\lambda_2}(z_1,\, z_2)\,, \tag{3.11}$$

with

$$\mathrm{M}_{0\lambda_2}(z_1,\, z_2) = \int \frac{d^2\underline{k}}{\underline{k}^2 (\underline{r} - \underline{k})^2}\, \mathrm{P_P}(\mathrm{z}_1, \underline{\mathrm{k}}, \underline{\mathrm{r}}, \mu_1)\, \underline{\mathrm{Q}}(\mathrm{z}_2, -\underline{\mathrm{k}}, -\underline{\mathrm{r}}, \mu_2) \cdot \underline{\epsilon}^{\lambda_2}\,; \tag{3.12}$$

for the case $\lambda_1 = +, -$:

$$\mathcal{M}_{\lambda_1 0} = i\, s\, \frac{C}{2}\, Q_2 \int_0^1 dz_1\, dz_2\, (z_1 - \bar{z}_1)\, \phi(z_1)\, z_2\, \bar{z}_2\, \phi(z_2) \mathrm{M}_{\lambda_1 0}(z_1,\, z_2)\,, \tag{3.13}$$

with

$$\mathrm{M}_{\lambda_1 0}(z_1,\, z_2) = \int \frac{d^2\underline{k}}{\underline{k}^2 (\underline{r} - \underline{k})^2}\, \underline{\mathrm{Q}}(\mathrm{z}_1, \underline{\mathrm{k}}, \underline{\mathrm{r}}, \mu_1) \cdot \underline{\epsilon}^{\lambda_1}\, \mathrm{P_P}(\mathrm{z}_2, -\underline{\mathrm{k}}, -\underline{\mathrm{r}}, \mu_2)\,. \tag{3.14}$$

and for the case $\lambda_1 = +, -\,, \lambda_2 = +, -$:

$$\mathcal{M}_{\lambda_1 \lambda_2} = i\, s\, \frac{C}{4} \int_0^1 dz_1\, dz_2\, (z_1 - \bar{z}_1)\, \phi(z_1)\, (z_2 - \bar{z}_2)\, \phi(z_2) \mathrm{M}_{\lambda_1 \lambda_2}(z_1,\, z_2)\,, \tag{3.15}$$

with

$$\mathrm{M}_{\lambda_1 \lambda_2}(z_1,\, z_2) = \int \frac{d^2\underline{k}}{\underline{k}^2 (\underline{r} - \underline{k})^2}\, \underline{\mathrm{Q}}(\mathrm{z}_1, \underline{\mathrm{k}}, \underline{\mathrm{r}}, \mu_1) \cdot \underline{\epsilon}^{\lambda_1 (1)}\, \underline{\mathrm{Q}}(\mathrm{z}_2, -\underline{\mathrm{k}}, -\underline{\mathrm{r}}, \mu_2) \cdot \underline{\epsilon}^{\lambda_2 (2)}\,. \tag{3.16}$$

Here and in the rest of this paper, we denote $C = 2\,\pi\, \frac{N_c^2 - 1}{N_c^2}\, \alpha_s^2\, \alpha_{em}\, f_\rho^2$. In terms of the above amplitudes, the corresponding differential cross-sections can be expressed in the large s limit (neglecting terms of order Q_i^2/s) as

$$\frac{d\sigma^{\gamma^*_{\lambda_1} \gamma^*_{\lambda_2} \to \rho^0_L \rho^0_L}}{dt} = \frac{|\mathcal{M}_{\lambda_1 \lambda_2}|^2}{16\,\pi\, s^2} \tag{3.17}$$

and it does not depend on s.

4 Non-forward Born order differential cross-section for $\gamma^*_{L,T}\,\gamma^*_{L,T} \to \rho^0_L\,\rho^0_L$

4.1 Analytical results for $k_\perp$-integrated amplitude $M_{\lambda_1\lambda_2}$

In this section we summarize the results for the amplitudes $M_{\lambda_1\lambda_2}$ obtained after performing analytically the $k_\perp$ integrals. Such analytic expressions give us the effective possibility of studying various kinematical limits in the variables Q_1^2, Q_2^2, t. The $k_\perp$ integrations were done using the method of Ref.[7] which exploits in an efficient way the scaling properties of integrals appearing in conformal field theories. The generic $k_\perp$ integral involves an integrand which corresponds to a box diagram with two distinct massive propagators and two massless propagators. Because of that, the $k_\perp$ integrations result in long and complicate expressions. Thus, we discuss below only the general structure of the results and we relegate all technical details of $k_\perp$ integrations to the Appendix.

In the transverse-transverse (TT) case, the amplitude can be expressed in term of two projection operators in the transverse plane as follows:

$$\mathrm{M}_{\lambda_1\lambda_2}(z_1,\,z_2) = \left[a(\underline{r};Q_1,Q_2;z_1,z_2)\left(\delta^{ij}-\frac{r^i r^j}{r^2}\right)+b(\underline{r};Q_1,Q_2;z_1,z_2)\frac{r^i r^j}{r^2}\right]\epsilon_i^{\lambda_1}\epsilon_j^{\lambda_2}\,, \quad (4.1)$$

where we denote $\underline{r}^2 = r^2$.

Combining (3.15) and (4.1), and using $|M_{++}|^2 = |M_{--}|^2$, one gets in the case of two photons with the same polarization :

$$|\mathcal{M}_{++}|^2 = |\mathcal{M}_{--}|^2 = s^2\,\frac{C^2}{64} \quad (4.2)$$
$$\times\left|\int_0^1 dz_1\,dz_2\,(z_1-\bar{z}_1)\,\phi(z_1)\,(z_2-\bar{z}_2)\,\phi(z_2)\;\left(b(\underline{r};Q_1,Q_2;z_1,z_2)-a(\underline{r};Q_1,Q_2;z_1,z_2)\right)\right|^2,$$

and analogously for different polarizations :

$$|\mathcal{M}_{+-}|^2 = s^2\,\frac{C^2}{64} \quad (4.3)$$
$$\times\left|\int_0^1 dz_1\,dz_2\,(z_1-\bar{z}_1)\,\phi(z_1)\,(z_2-\bar{z}_2)\,\phi(z_2)\;\left(b(\underline{r};Q_1,Q_2;z_1,z_2)+a(\underline{r};Q_1,Q_2;z_1,z_2)\right)\right|^2.$$

For the longitudinal-transverse (LT) case, restoring the dependency over all variables, one defines from (3.12) and (3.14) the scalar function f

$$\mathrm{M}_{0\lambda}(\underline{r};Q_1,Q_2;z_1,\,z_2) = f(\underline{r};Q_1,Q_2;z_1,\,z_2)\,\underline{r}\cdot\underline{\epsilon}^{\,\lambda}\,, \quad (4.4)$$

or equivalently

$$\mathrm{M}_{\lambda 0}(\underline{r};Q_1,Q_2;z_1,\,z_2) = f(\underline{r};Q_2,Q_1;z_2,\,z_1)\,\underline{r}\cdot\underline{\epsilon}^{\,\lambda}\,, \quad (4.5)$$

which leads to

$$|\mathcal{M}_{0+}|^2 = |\mathcal{M}_{0-}|^2 = s^2\,\frac{C^2}{8}\,Q_1^2\,\underline{r}^2\,\left|\int_0^1 dz_1\,dz_2\,z_1\,\bar{z}_1\,\phi(z_1)\,(z_2-\bar{z}_2)\,\phi(z_2) f(\underline{r};Q_1,Q_2;z_1,\,z_2)\right|^2 . \tag{4.6}$$

and analogously for the transverse-longitudinal (TL) case

$$|\mathcal{M}_{+0}|^2 = |\mathcal{M}_{-0}|^2 = s^2\,\frac{C^2}{8}\,Q_2^2\,\underline{r}^2\,\left|\int_0^1 dz_1\,dz_2\,z_2\,\bar{z}_2\,\phi(z_2)\,(z_1-\bar{z}_1)\,\phi(z_1) f(\underline{r};Q_2,Q_1;z_2,\,z_1)\right|^2 . \tag{4.7}$$

The expressions of $a(\underline{r};Q_1,Q_2;z_1,z_2)$, $b(\underline{r};Q_1,Q_2;z_1,z_2)$ and $f(\underline{r};Q_1,Q_2;z_1,\,z_2)$ presented as combinations of *finite* standard integrals are given in the Appendix.

For the longitudinal-longitudinal (LL) case, it turned out [7] that (3.9) can be effectively replaced by $\tilde{M}(z_1,\,z_2)$ whose integral over $z_{1,2}$ with symmetrical DA gives the same result. $\tilde{M}(z_1,\,z_2)$ reads

$$\begin{aligned}\tilde{M}_{00}(z_1,\,z_2) = &-\left(\frac{1}{z_1^2\underline{r}^2+\mu_1^2}+\frac{1}{\bar{z}_1^2\underline{r}^2+\mu_1^2}\right)J_{3\mu_2}(z_2)-\left(\frac{1}{z_2^2\underline{r}^2+\mu_2^2}+\frac{1}{\bar{z}_2^2\underline{r}^2+\mu_2^2}\right)J_{3\mu_1}(z_1)\\ &+J_{4\mu_1\mu_2}(z_1,\,z_2)+J_{4\mu_1\mu_2}(\bar{z}_1,\,z_2)\,.\end{aligned} \tag{4.8}$$

$J_{3\mu}$ and $J_{4\mu_1\mu_2}$ are two dimensional integrals with respectively 3 propagators (1 massive) and 4 propagators (2 massive, with different masses), they are both IR and UV finite. Their expressions are given in the Appendix.

Due to the collinear conformal subgroup $SL(2,R)$ invariance [17], the ρ_L^0 distribution amplitude has an expansion in terms of Gegenbauer polynomials of even order which reads

$$\phi(z) = 6z(1-z)\,(1+\sum_{n=1}^{\infty} a_{2\,n} C_{2\,n}^{3/2}(2z-1))\,. \tag{4.9}$$

Except for a short discussion in section 5.3, we restrict ourselves to the asymptotical distribution amplitude corresponding to $a_{2\,n}=0$.

To complete the evaluation of the amplitude $\mathcal{M}$, one needs to integrate over the quark momentum fractions z_1 and z_2 in the ρ mesons. For arbitrary values of t, it seems not possible to perform the z_1 and z_2 integrations analytically. We thus do them numerically. We observe the absence of end-point singularity when $z_{1(2)}\to 0$ or $z_{1(2)}\to 1$. Indeed, for the longitudinal polarizations involving P_P as defined in Eq.(3.4), the z divergency of type $1/z$, $1/(1-z)$ is compensated by the $z\bar{z}$ factor when $z\to 0$, 1, while for transverse polarizations, involving $\underline{Q}$ as defined in Eq.(3.6), there is no singularity since $\underline{Q}$ is itself regular.

For the special case $t=t_{min}$ (where only the LL amplitude is non-vanishing), which will be useful in the discussion of sections 4.2 and 5.3, the integration over z_i can be performed analytically, with the result [7]

$$\mathcal{M}_{00} = -is\,\frac{N_c^2-1}{N_c^2}\,\alpha_s^2\,\alpha_{em}\,f_\rho^2\,\frac{9\pi^2}{2}\,\frac{1}{Q_1^2Q_2^2}\left[6\,\left(R+\frac{1}{R}\right)\ln^2 R+\,12\,\left(R-\frac{1}{R}\right)\ln R\right.$$

$$+12\left(R+\frac{1}{R}\right)+\left(3\,R^2+2+\frac{3}{R^2}\right)\left(\ln(1-R)\,\ln^2 R-\ln(R+1)\,\ln^2 R\right.$$
$$\left.-2\,\mathrm{Li}_2(-R)\,\ln R+2\,\mathrm{Li}_2(R)\,\ln R+2\,\mathrm{Li}_3(-R)-2\,\mathrm{Li}_3(R)\right)], \tag{4.10}$$

where $R = Q_1/Q_2$. When $Q_1 = Q_2$, the expression (4.10) simplifies to

$$\mathcal{M}_{00} = is\frac{N_c^2-1}{N_c^2}\,\alpha_s^2\alpha_{em}f_\rho^2\,\frac{9\pi^2}{Q^4}(14\zeta(3)-12)\,. \tag{4.11}$$

4.2 Results for differential cross-section

The formulae for $\mathrm{M}_{\lambda_1\lambda_2}$ obtained in sec.4 permit us to evaluate the magnitudes of cross-sections (3.17) of the diffractive double rho production for different helicities of virtual photons. In our estimates we use as a strong coupling constant the three-loop running $\alpha_S(Q_1Q_2)$ with $\Lambda^{(4)}_{\overline{MS}} = 305\,\mathrm{MeV}$ (see, e.g. [18]).[2]

In Fig.5 we display the t-dependence of the different $\gamma^*_{L,T}\;\gamma^*_{L,T} \to \rho^0_L\;\rho^0_L$ differential cross-sections for various values of $Q = Q_1 = Q_2$.

We first note the strong decrease of all the cross-sections when $Q^2_{1,2}$ increase. For LL, this follows from an obvious dimensional analysis, since

$$\mathcal{M}_{LL} \propto \frac{s\,f_\rho^2}{Q^4}$$

(for $Q_1 = Q_2 = Q$), in agreement with (4.11).

Secondly, all the differential cross-sections which involve at least one transverse photon vanish when $t = t_{min}$. It is due to the vanishing of the function $\underline{Q}$ for $\underline{r} = 0$ (see (3.6)). Physically, this fact is related to the s-channel helicity conservation at $t = t_{min}$. Indeed, since the t-channel gluons carry non-sense polarizations, helicity conservation occurs separately in each impact factor.

In Fig.6, we show the shape of the integrands $\overline{\mathrm{M}}_{\lambda_1,\lambda_2}$ of the various amplitudes $\mathcal{M}_{\lambda_1\lambda_2}$ as a function of z_1 and z_2, as they appear in formulas (3.11, 3.13 and 3.15):

$$\overline{\mathrm{M}}_{00} = z_1\,\bar z_1\,\phi(z_1)\,z_2\,\bar z_2\,\phi(z_2)\,\mathrm{M}_{00}(z_1,\,z_2)\,, \tag{4.12}$$

and for $\lambda_i = +,-$

$$\overline{\mathrm{M}}_{\lambda_1 0} = (z_1-\bar z_1)\,\phi(z_1)\,z_2\,\bar z_2\,\phi(z_2)\,\mathrm{M}_{\lambda_1 0}(z_1,\,z_2)\,, \tag{4.13}$$
$$\overline{\mathrm{M}}_{\lambda_1\lambda_2} = (z_1-\bar z_1)\,\phi(z_1)\,(z_2-\bar z_2)\,\phi(z_2)\,\mathrm{M}_{\lambda_1\lambda_2}(z_1,\,z_2)\,. \tag{4.14}$$

$\mathrm{M}_{\lambda_1\lambda_2}(z_1,\,z_2)$ is symetric under $(z_i \leftrightarrow \bar z_i)$ for a longitudinal polarization $\lambda_i = 0$ (cf. 3.4) and antisymetric under $(z_i \leftrightarrow \bar z_i)$ for a transverse polarization $\lambda_i = +,-$ (cf. 3.6); thus the factors $z_i\,\bar z_i$ for $\lambda_i = 0$ and $z_i - \bar z_i$ for $\lambda_i = +,-$ ensure the symmetry of $\overline{\mathrm{M}}_{\lambda_1\lambda_2}$ under

[2]Running of α_S is in principle a subleading effect with respect to our treatment. Nevertheless, numerically, as we discuss in sec.5.3, the dependence of our predictions for the rates in e^+e^- scattering on a choice of α_s is negligible at Born order, but is more subtle when LO BFKL corrections are taken into account.

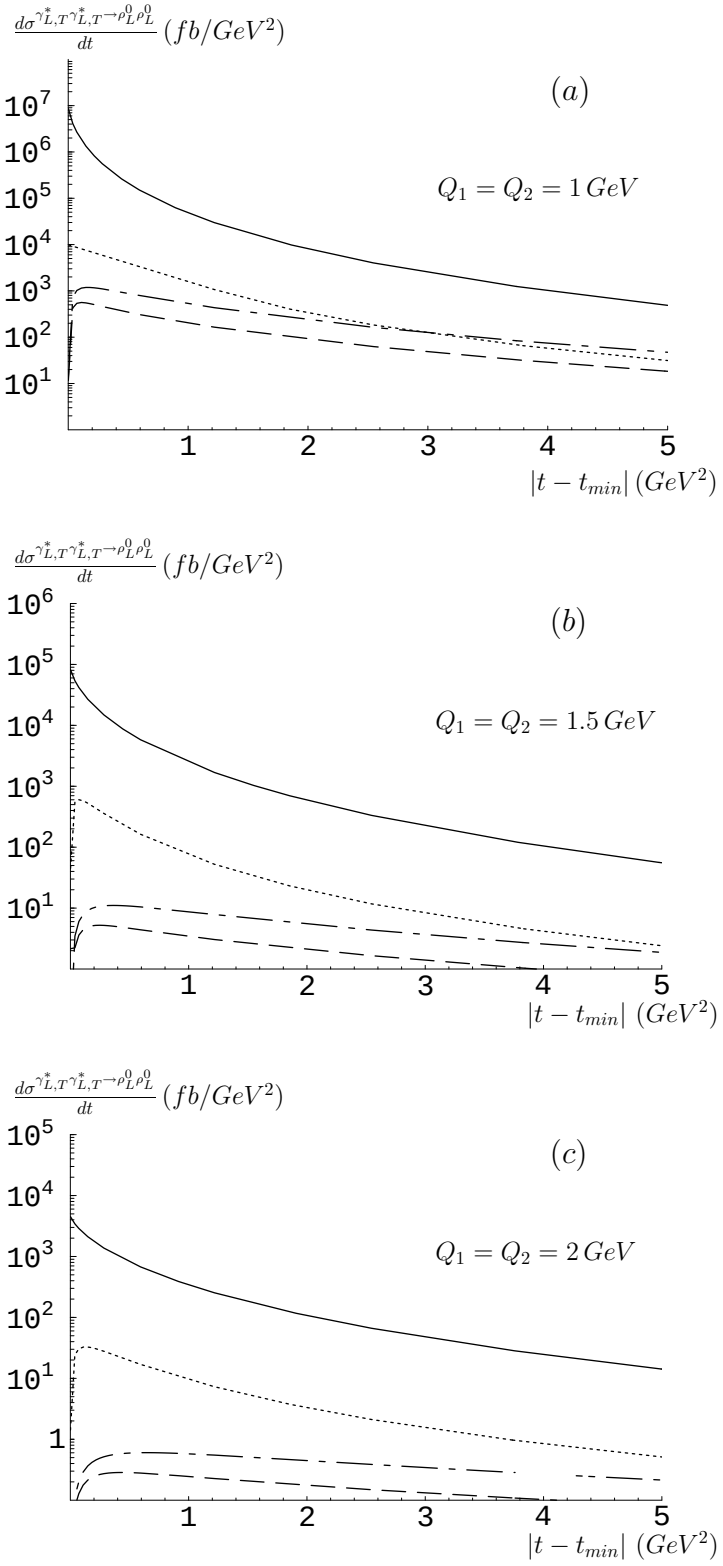

Figure 5: Differential cross-sections for the process $\gamma^*_{L,T}\ \gamma^*_{L,T} \to \rho^0_L\ \rho^0_L$. The solid curve corresponds to the $\gamma^*_L\gamma^*_L$ mode, the dotted one to the $\gamma^*_L\gamma^*_T$ mode, the dashed and the dashed-dotted ones to the $\gamma^*_T\gamma^*_{T'}$ modes with respectively the same $T = T'$ and different $T \neq T'$ transverse polarizations. The different figures (a), (b), (c) correspond to different values of $Q_1 = Q_2$.

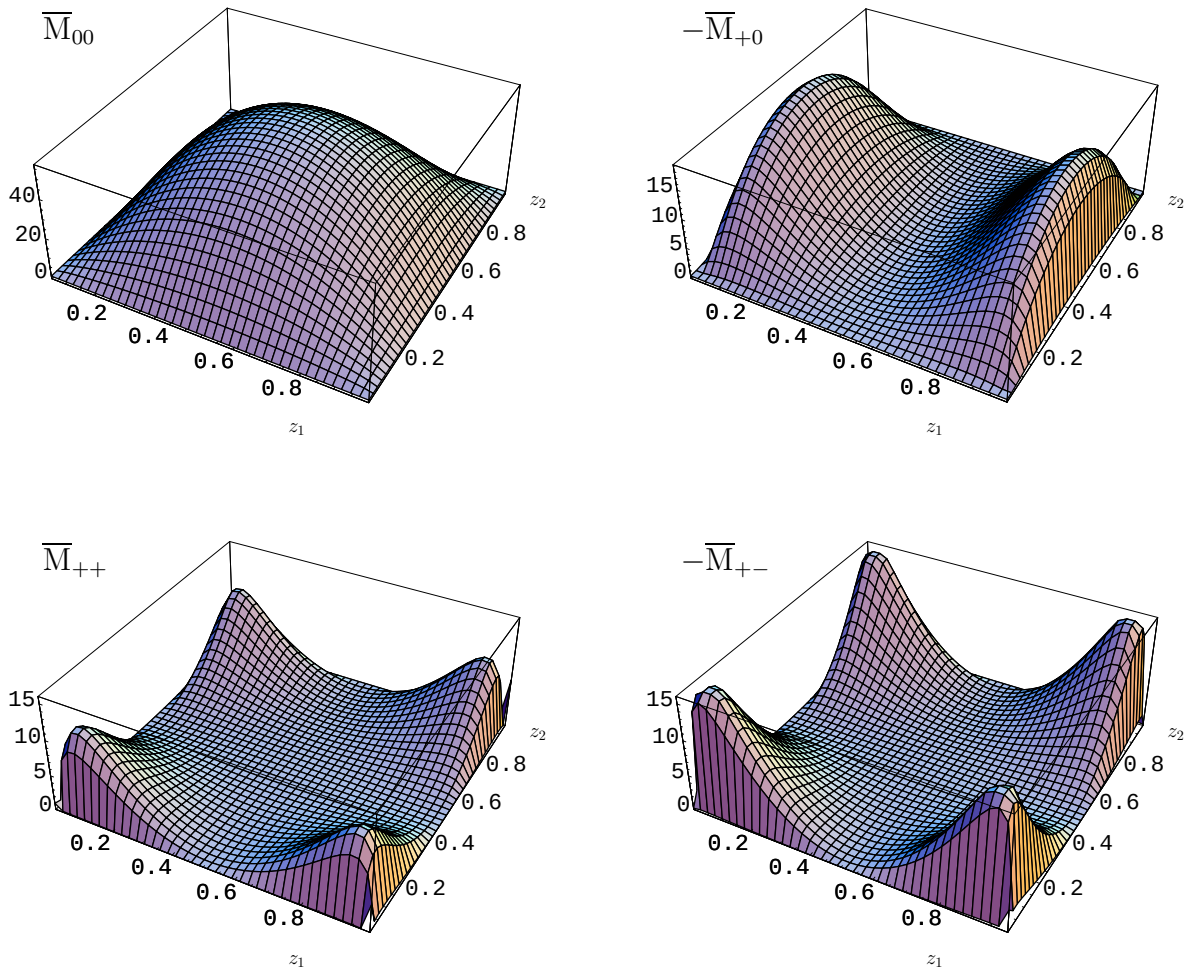

Figure 6: Shape of the amplitudes $\overline{\mathrm{M}}_{00}$, $-\overline{\mathrm{M}}_{+0}$, $\overline{\mathrm{M}}_{++}$, $-\overline{\mathrm{M}}_{+-}$ as functions of z_1 and z_2, for $-t = 0.16\,\mathrm{GeV}^2$ and $Q_1 = Q_2 = 1\,\mathrm{GeV}$.

($z_i \leftrightarrow \bar{z}_i$) as we can see on Fig.6. Because of the ρ^0_L mesons distribution amplitudes $\phi(z_i)$, $\overline{\mathrm{M}}_{\lambda_1\lambda_2}(z_1,\, z_2)$ vanishes for any polarization in the end-point region. Consequently the case of a transverse polarization vanishes in the central region $z_i = \bar{z}_i = 1/2$ and also in the end-point region z_i close to 0 or 1, so that it restricts the available z_i phase-space and reduces the resulting differential cross-section, in agreement with the dominance of longitudinal photons (helicity conservation) in the process $\gamma^*_{L,T}\,\gamma^*_{L,T} \to \rho^0_L\,\rho^0_L$.

The amplitude involving at least one transverse photon has a maximum at low $-t$ value with respect to Q_1Q_2. The Fig.6 corresponds to $-t = 0.16$ GeV^2 which is a typical value for the region where the cross-sections with transverse photons in Fig.5 are maximal.

A peculiarly characteristic shape appears in the amplitudes with two transverse photons, as shown in bottom panels of Fig.6. When the value of t changes towards t_{min} the peaks become very narrow, as shown in the left panel in Fig.7 for $\overline{\mathrm{M}}_{+-}$. For t very close to t_{min} they are practically concentrated only on the boundary which leads to the vanishing of the amplitude. On the other hand, when the value of t increases and leaves

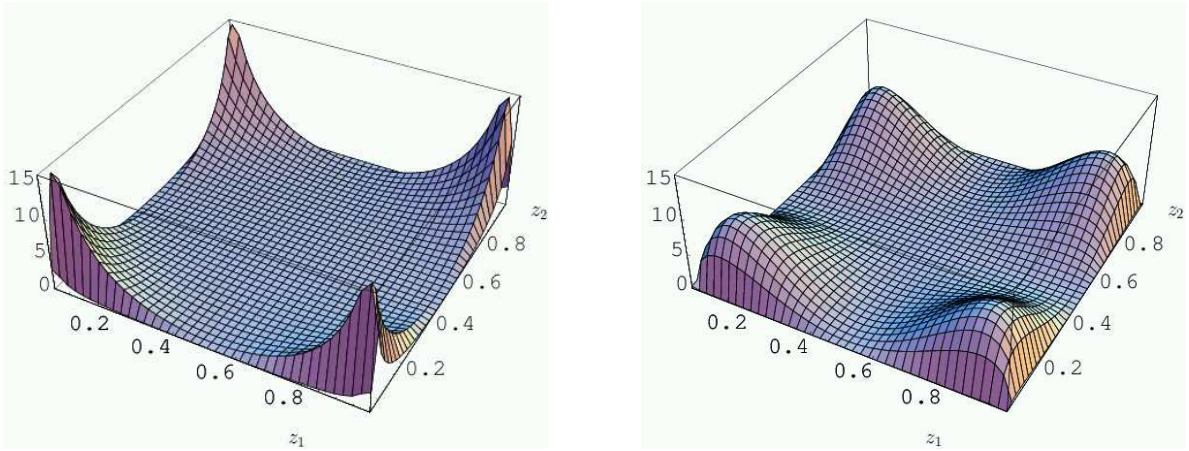

Figure 7: Shape of the amplitude $-\overline{\mathrm{M}}_{+-}$, for $-t = 0.01\,\mathrm{GeV}^2$ (left) and $-t = 0.8\,\mathrm{GeV}^2$ (right), with $Q_1 = Q_2 = 1\,\mathrm{GeV}$.

the maximum of cross-sections the peaks in Fig.6 decrease and spread, as shown for $\overline{\mathrm{M}}_{+-}$ in the right panel of Fig.7.

In the case of LT polarizations, the shape of the amplitude $\overline{\mathrm{M}}_{+0}$, which contains only one factor $(z_i - \bar{z}_i)$, is shown in the right upper panel of Fig.6. Its comparison with the upper left panel of Fig.6, showing the shape of the $\overline{\mathrm{M}}_{00}$ amplitude, leads to the conclusion that $\overline{\mathrm{M}}_{+0}$ shares some properties with $\overline{\mathrm{M}}_{+-}$ and $\overline{\mathrm{M}}_{00}$. In particular, the presence of a transverse polarization leads to the vanishing of $\overline{\mathrm{M}}_{+0}$ at $t = t_{min}$. On the other hand, the presence of a longitudinal polarization increases the cross-section at small values of t. As a consequence of the competition of these two mechanisms, the maximum of the cross-section determined by $\overline{\mathrm{M}}_{+0}$ is located closer to t_{min} than in the case of the cross-section given by $\overline{\mathrm{M}}_{+-}$. This is illustrated in Fig.8 which shows the t-dependence of the various differential cross-sections in log-log scale.

Third, in Fig.9, we display the t-dependence of the $\gamma^*_{L,T}\ \gamma^*_{L,T} \to \rho^0_L\ \rho^0_L$ differential cross-sections for $Q = Q_1 = Q_2 = 1$ GeV up to values of $-t$ much larger than photon virtualities Q_i, where t plays the role of the dominant hard scale in our process. Of course, in such a kinematical region the cross-section are strongly suppressed in comparison with the small t one. Nevertheless, Fig.9 illustrates the expected fact that the hierarchy of cross-sections is different in two regions: at large t, the $\gamma^*_T\ \gamma^*_T \to \rho^0_L\ \rho^0_L$ cross-section dominates over the one of $\gamma^*_L\ \gamma^*_L \to \rho^0_L\ \rho^0_L$, which is the dominant cross-section at small t, since the virtual photons are almost on shell with respect to the large scale given by t.

To conclude this subsection, we note that all the above cross-sections are strongly peaked in the forward cone. The phenomenological predictions obtained in the region of the forward cone will practically dictate the general trends of the integrated cross-sections. This fact is less dangerous than for the real photon case since the virtual photon is not in the direction of the beam, and thus the outgoing ρ mesons can be tagged. The only difficulty has to do with the tagging of the outgoing lepton, since the cross-section is dominated by small (hard) values of $Q^2_{1,2}$. In this section we did not modify cross-sections by taking into account the virtual photon fluxes, which would amplify both, the dominance

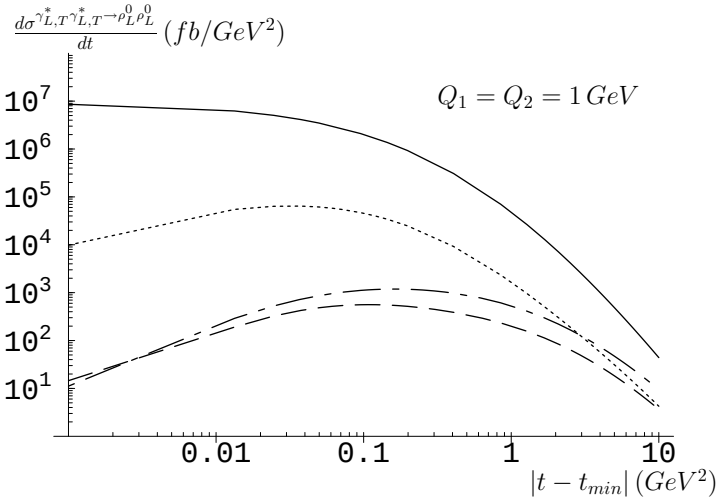

Figure 8: Differential cross-sections for the process $\gamma^*_{L,T}\ \gamma^*_{L,T} \to \rho^0_L\ \rho^0_L$, for small value of t. The solid curve corresponds to the $\gamma^*_L\gamma^*_L$ mode, the dotted one to the $\gamma^*_L\gamma^*_T$ mode, the dashed and the dashed-dotted ones to the $\gamma^*_T\gamma^*_{T'}$ modes with respectively the same $T = T'$ and different $T \neq T'$ transverse polarizations, for $Q_1 = Q_2 = 1\,\mathrm{GeV}$.

of small Q^2 region as well as the small y_i domain, characteristic for very forward outgoing leptons. This is discussed in section 5. In particular, it will be shown that the differential cross-sections are experimentaly visible and seems to be sufficient for the $t-$dependence to be measured up to a few GeV^2.

Note also that at this level of calculation there is no s-dependence of the cross-section. It will appear after taking into account triggering effects and/or BFKL evolution.

4.3 Quark exchange contribution to the cross-section

The process (1.3) described above involves gluon exchanges which dominate at high energies. However, at lower energy, the process can be described by double quark exchange. This was investigated in [9], in the case $t = t_{min}$. Fig.10 shows in particular the diagrams which contributes to the amplitude M_H (see Fig.2) for the process $\gamma^*_L(q_1)\ \gamma^*_L(q_2) \to \rho_L(k_1)\ \rho_L(k_2)$. Using the Eqs.(12) and (13) of [9] together with the asymptotical ρ^0_L distribution amplitude (4.9) one obtains the scattering amplitude for the photons longitudinally polarized

$$\mathcal{M}^{q\bar{q}}_{00} = -\,40\,\pi^2\,\frac{N_c^2-1}{N_c^2}\,\frac{\alpha_s\,\alpha_{em}\,f_\rho^2}{s}\left[1+\frac{\left(1+\frac{Q_1^2}{s}+2\frac{Q_1^2}{s}\frac{\ln\frac{Q_1^2}{s}}{1-\frac{Q_1^2}{s}}\right)\left(1+\frac{Q_2^2}{s}+2\frac{Q_2^2}{s}\frac{\ln\frac{Q_2^2}{s}}{1-\frac{Q_2^2}{s}}\right)}{\left(1-\frac{Q_1^2}{s}\right)\left(1-\frac{Q_2^2}{s}\right)}\right] \tag{4.15}$$

and for the transversally polarized photons

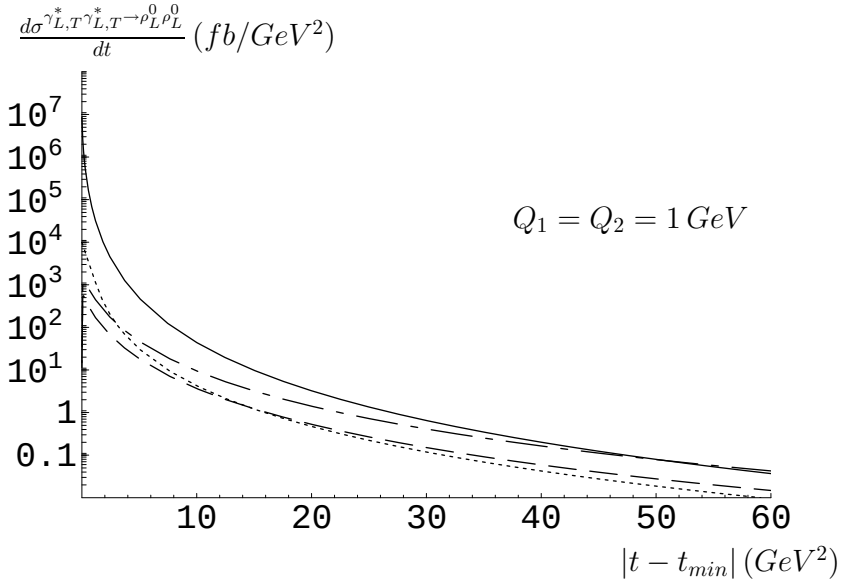

Figure 9: Differential cross-sections for the process $\gamma^*_{L,T}\,\gamma^*_{L,T} \to \rho^0_L\,\rho^0_L$, up to asymptotically large t. The solid curve corresponds to the $\gamma^*_L\gamma^*_L$ mode, the dotted one to the $\gamma^*_L\gamma^*_T$ mode, the dashed and the dashed-dotted ones to the $\gamma^*_T\gamma^*_{T'}$ modes with respectively the same $T = T'$ and different $T \neq T'$ transverse polarizations, for $Q_1 = Q_2 = 1\,\mathrm{GeV}$.

$$\begin{aligned}
\mathcal{M}^{q\bar{q}}_{TT} &= \mathcal{M}^{q\bar{q}}_{++} + \mathcal{M}^{q\bar{q}}_{--} \qquad (4.16)\\
&= -\,40\,\pi^2\,\frac{N_c^2-1}{N_c^2}\,\frac{\alpha_s\,\alpha_{em}\,f_\rho^2}{s}\,\frac{\left(\frac{7}{2}+\frac{2\left(1+\frac{Q_1^2}{s}\right)\ln\frac{Q_1^2}{s}}{1-\frac{Q_1^2}{s}}\right)\left(\frac{7}{2}+\frac{2\left(1+\frac{Q_2^2}{s}\right)\ln\frac{Q_2^2}{s}}{1-\frac{Q_2^2}{s}}\right)-\frac{1}{4}}{\left(1-\frac{Q_1^2}{s}\right)\left(1-\frac{Q_2^2}{s}\right)}.
\end{aligned}$$

In the large s limit, one respectively gets

$$\mathcal{M}^{q\bar{q}}_{00} \simeq -\,80\,\pi^2\,\frac{N_c^2-1}{N_c^2}\,\frac{\alpha_s\,\alpha_{em}\,f_\rho^2}{Q_1\,Q_2} \qquad (4.17)$$

and

$$\begin{aligned}
\mathcal{M}^{q\bar{q}}_{TT} &\simeq -\,40\,\pi^2\,\frac{N_c^2-1}{N_c^2}\,\frac{\alpha_s\,\alpha_{em}\,f_\rho^2}{s}\left(4\ln\frac{Q_1^2}{s}\,\ln\frac{Q_2^2}{s}+14\,\ln\frac{Q_1\,Q_2}{s}+12\right) \qquad (4.18)\\
&= -\,40\,\pi^2\,\frac{N_c^2-1}{N_c^2}\,\frac{\alpha_s\,\alpha_{em}\,f_\rho^2}{s}\left(4\ln^2\frac{Q_1\,Q_2}{s}+14\,\ln\frac{Q_1\,Q_2}{s}-4\,\ln^2 Q_1/Q_2+12\right).
\end{aligned}$$

Other amplitudes vanish at $t = t_{min}$.

These expressions should be compared with the corresponding 2 gluons exchange contributions discussed in the previous sections. The LL amplitude is almost constant around $t = t_{min}$, and given by (4.10).

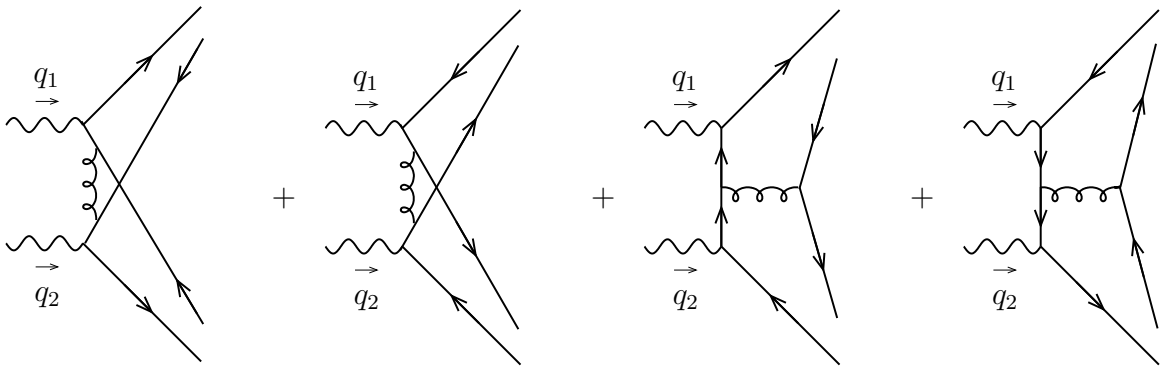

Figure 10: Feynman diagrams contributing to M_H in the case of longitudinally polarized virtual photons.

The TT amplitude (4.1) behaves as

$$\mathcal{M}_{TT}^{gg} \simeq -i\, a\, \frac{\pi}{2}\, s\, \frac{N_c^2-1}{N_c^2}\, \alpha_s^2\, \alpha_{em}\, f_\rho^2\, \frac{|t-t_{min}|}{Q_1^3 Q_2^3}\,, \tag{4.19}$$

where the constant $a = 253.5$ is extracted from a numerical fit.

The Eqs. (4.15 - 4.19) confirm the well known fact that in the Regge limit the two gluon exchange dominates over the double quark exchange. Indeed, the comparison of expressions (4.17) and (4.18) with formulas (4.10) and (4.19) shows that gluonic contributions are proportional to s (in agreement with the usual counting rule $s^{\Sigma\sigma_i - N + 1}$, where N is the number of t channel exchanged particles of spin σ_i). In the case of longitudinally polarized photons which does not vanish at t_{min}, and for the same photon virtualities $Q_1^2 = Q_2^2 = Q^2$, let us consider the ratio

$$\mathcal{R}_{LL} = \frac{\mathcal{M}_{00}^{q\bar{q}}}{\mathcal{M}_{00}^{gg}} = \frac{32\,(Q_u^2 + Q_d^2)}{28\,\zeta(3) - 24}\, \frac{Q^2}{s\,\alpha_s}\,. \tag{4.20}$$

For a typical value of $Q^2 = 1$ GeV^2, as soon as s ($\simeq s_{\gamma^*\gamma^*}$) is higher than 4 GeV^2, this ratio is bigger than unity, which at first sight seems to be always the case for ILC. (4.10) would thus completely dominates with respect to (4.15), by several orders of magnitudes. In fact, $s_{\gamma^*\gamma^*}$ can reach such low value as 4 GeV^2, because of the outgoing energy carried by the outgoing leptons and the strong peak of the Weizsäcker-Williams fluxes at small γ^* energies. We discuss this effect in section 5.3 at the level of the e^+e^- process, after performing the phase-space integration of the differential cross-section at t_{min}. It will be shown that nevertheless the quark contribution is really negligible in almost all the ILC phase space.

In the case of the two gluon contribution with transverse virtual photons (4.19) which vanishes at $t = t_{min}$, its dominance over the corresponding quark contribution (4.16) appears very rapidly when $|t - t_{min}|$ starts to increase, and persists in the whole essential region of the phase space (remember that (4.19) is peaked at $t - t_{min} = k\ 0.01$GeV^2 where

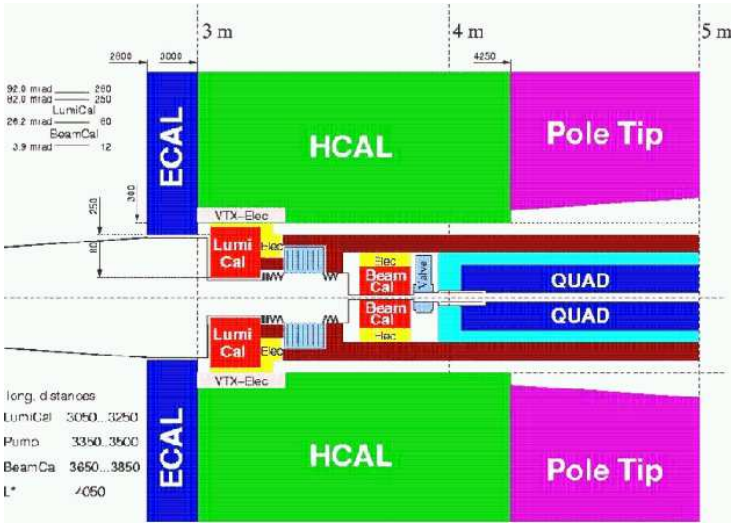

Figure 11: The LDC project, with the BeamCal forward electromagnetic calorimeter.

k is of order 1-10). This dominance will also be discussed in more detail in section 5.3 at the level of the e^+e^- process.

5 Non-forward Born order cross-section for $e^+e^- \to e^+e^-\rho_L^0\,\rho_L^0$

5.1 Kinematical cuts for the phase-space integration

Our purpose is now to evaluate the cross-section of the process $e^+e^- \to e^+e^-\rho_L^0\,\rho_L^0$ in the planned experimental conditions of the International Linear Collider project [19]. For the detector part, we chose to focus on the Large Detector Concept [20], and use the potential of the very forward region accessible through the electromagnetic calorimeter BeamCal which may be installed around the beampipe at 3.65 m from the interaction point. The LDC is illustrated in Fig.11.

The cross-section which takes into account all the kinematical constraints, which are explained below, is given by

$$\frac{d\sigma^{e^+e^-\to e^+e^-\rho_L\rho_L}}{dt} = \int_{Q^2_{1min}}^{Q^2_{1max}} dQ_1^2 \int_{Q^2_{2min}}^{Q^2_{2max}} dQ_2^2 \int_{\epsilon}^{y_{max}} dy_1 \int_{\frac{Q_1Q_2}{sy_1}}^{y_{max}} dy_2 \, \frac{d\sigma^{e^+e^-\to e^+e^-\rho_L\rho_L}}{dt\, dy_1\, dy_2\, dQ_1^2\, dQ_2^2}\,, \quad (5.1)$$

with $Q_{1min} = 1$ GeV, $Q_{1max} = 4$ GeV, $\epsilon = 10^{-6}$ and $y_{max} = 0.6$.

The cross-section (5.1) can be evaluated combining the cross-section formulae (2.2), (3.17) and the results of section 4.2 for the helicity scattering amplitudes.

The important feature of the formula (5.1) is that the dominant contribution for the $e^+\,e^- \to e^+\,e^-\,\rho_L^0\,\rho_L^0$ process is strongly peaked at low Q_i. The integration over Q_i, y_i is peaked in the low y_i and Q_i phase space region due to the presence in (2.2) of $1/(y_i\,Q_i^2)$ factors coming from the Weizsäcker-Williams fluxes, and thus amplifies this effect. We

show below that this dominant part of the phase space is accessible experimentaly using the BeamCal calorimeter.

The integration domain in (5.1) is fixed by the following considerations. In the laboratory frame, which is also the center of mass system (cms) for a linear collider, the standard expression for the momentum fractions which respect to the incoming leptons and for the virtualities of the bremsstrahlung photons are, respectively, given by

$$y_i = \frac{E - E_i' \cos^2(\theta_i/2)}{E} \quad \text{and} \quad Q_i^2 = 4EE_i' \sin^2(\theta_i/2)\,, \tag{5.2}$$

where E is the energy of the beam, while E_i' and θ_i are respectively the energy and the scattering angle of the out-going leptons. At ILC, the foreseen cm energy is $\sqrt{s} = 2E = 500$ GeV. The experimental constraint coming from the minimal detection angle θ_{min} around the beampipe is given by $\theta_{max} = \pi - \theta_{min} > \theta_i > \theta_{min}$ and leads to the following constraint on y_i

$$y_i > f(Q_i) = 1 - \frac{Q_i^2}{s \tan^2(\theta_{min}/2)}\,, \tag{5.3}$$

where the constraint on the upper bound of y_i coming from θ_{max} is completely negligible at this cm energy.
The condition on the energy of the scattered lepton $E_{max} > E_i' > E_{min}$ results in

$$y_{i\,max} = 1 - \frac{E_{min}}{E} > y_i > 1 - \frac{E_{max}}{E}. \tag{5.4}$$

Moreover we impose that $s_{\gamma^*\gamma^*} = y_1 y_2 s > c\,Q_1\,Q_2$ (where c is an arbitrary constant of the order 1) which is required by the Regge kinematics for which the impact representation is valid. In subsection 5.3 we show that this constant c can be adjusted to choose bins of data for which also in the case of e^+e^- scattering the contribution with quark exchanges (discussed in sec.4.3) is completely negligible.

We arbitrarily choose Q_i to be bigger than 1 GeV as it provides the hard scale of the process which legitimates the use of perturbation theory. $Q_{i\,max}$ will be fixed to 4 GeV, since the various amplitudes involved are completely negligible for higher values of virtualities Q_i values (see section 4.2). The constraints on $y_{i\,min}$ discussed so far are summarized by conditions

$$y_{1\,min} = \max\left(f(Q_1), 1 - \frac{E_{max}}{E}\right) \text{ and } y_{2\,min} = \max\left(f(Q_2), 1 - \frac{E_{max}}{E}, \frac{c\,Q_1\,Q_2}{s\,y_1}\right)\,. \tag{5.5}$$

Further simplifications of conditions (5.5) can be done by taking into account that the only condition on the maximal value of energy detection of the scattered leptons comes from kinematics, i.e. $E_{max} = E$, and some specific features of the planned detector.

The BeamCal calorimeter in the very forward region allows in principle to detect particles down to 4 mrad.[3] More precisely, it measures an energy deposit for an angle between 4 mrad and 26 mrad. But this detector is also polluted by the photon beamstrahlung,

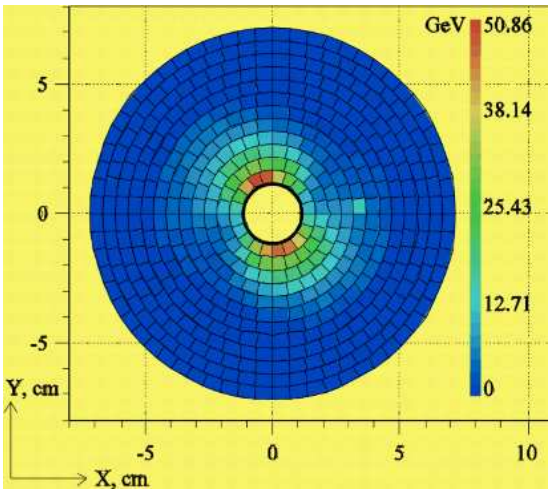

Figure 12: Energy deposit in GeV in each cell of the BeamCal detector due to beamstrahlung.

specialy for very small angles (see Fig.12). We assume a non ambiguous identification for particles whose energies are bigger than 100 GeV. More precisely, the efficiency of detection of an electron depends on its energy and becomes less ambiguous when the energy increases. It is above 70 % in the part of the phase space which dominates the cross-section (small y_i, corresponding to $E_i' \simeq E_i$). A precise evaluation of this efficiency would require to set up a Monte Carlo simulation for the beamstrahlung contribution, which is beyond the scope of this paper. This sets the maximal value of y_i to $y_{i\,max} = 1 - \frac{E_{min}}{E} = 0.6$ with $E_{min} = 100$ GeV and $E = 250$ GeV.

Such a big value of E_{min} can be considered as surprisingly high and could lead to a strong reduction of the allowed phase space. In principle one could enlarge the phase space by taking into account particles whose energies E_i' are between 100 GeV and 20 GeV with angles θ_i bigger than 10 mrad (see Fig.12), but the contribution of this domain is negligible (see Fig.13) since the lower bound of y_i (see Eq.(5.5)) prevents us to reach the small values of y_i and Q_i which give the dominant contribution to the cross-section. We safely neglect the contribution of this region of phase space and assume in the following $E_{min} = 100$ GeV and $\theta_{min} = 4$ mrad.

Thus, with $\theta_{min} = 4$ mrad and $\sqrt{s} = 500$ GeV, we have $s \tan^2(\theta_{min}/2) = 1\,\mathrm{GeV}^2$, which means that $f(Q) \leq 0$ for $Q^2 \geq 1\mathrm{GeV}^2$. The relations (5.5), with $E_{max} = E$, reduce to only one condition $y_{2min} = \frac{Q_1 Q_2}{s y_1}$. This has to be supplemented numerically with the condition $y_{1min} = \epsilon$, where ϵ is a numerical cut-off: although, because of the Regge limit condition, we have $y_1 > \frac{Q_1 Q_2}{s y_2} \geq \frac{Q_{1min} Q_{2min}}{s y_{2max}} = 6.610^{-6}$ which thus provides a natural lower cut-off for y_1, nevertheless we choose $\epsilon = 10^{-6}$ so that it is smaller than the smallest reachable value of y_1 but still non zero. This cut-off has no practical effect, except for avoiding numerical instabilities in the integration code.

The above discussion justifies the various cuts in formula (5.1).

[3]Note that in order to get access to any inclusive [4] or diffractive high s processes, one needs very small θ_{min}. To reach values of θ_{min} of a few mrads represents an important technological step which was not feasible a few years ago.

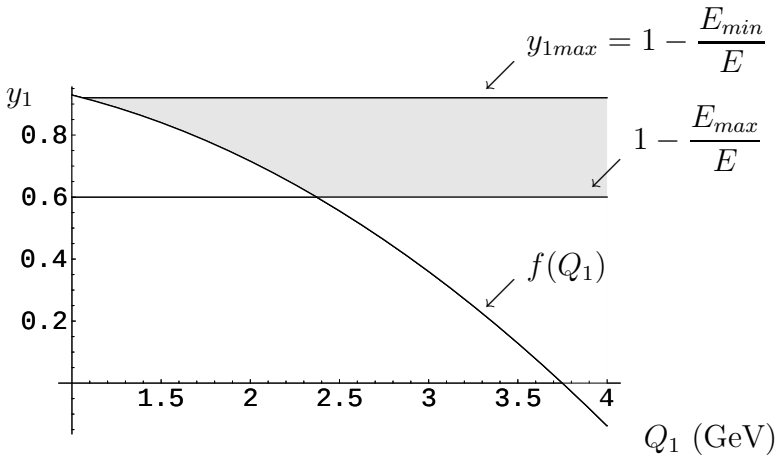

Figure 13: y_1 integration domain for $\theta_{min} = 10$ mrad, $E_{min} = 20\,\text{GeV}$ and $E_{max} = 100\,\text{GeV}$.

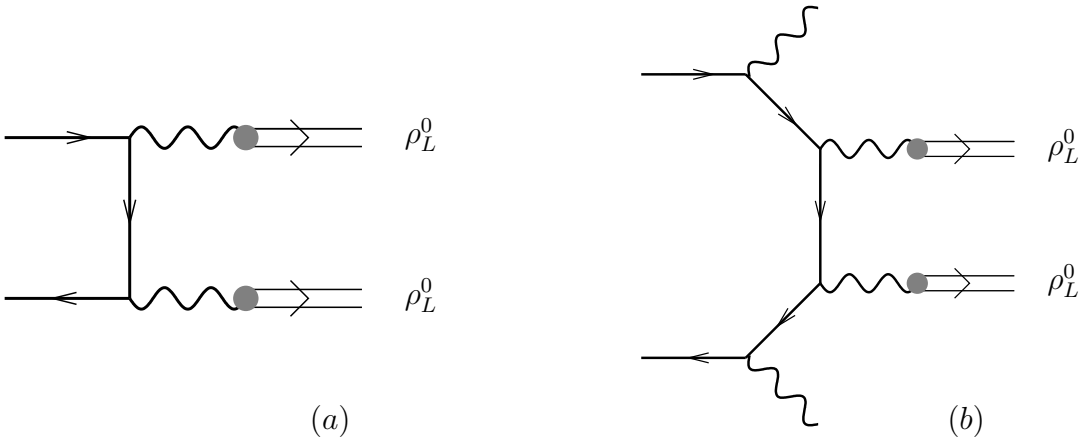

Figure 14: Example of Born order diagrams for the process $e^+e^- \to \rho_L^0\ \rho_L^0$ (a) and for the $e^+e^- \to \gamma\,\gamma\,\rho_L^0\ \rho_L^0$ process (b).

5.2 Background in the detector

BeamCal is an electromagnetic calorimeter which cannot distinguish charges of particles. Thus, it is important to check that the cross-sections of any other processes which could lead to final states which can be misidentified with the final state of the process $e^+e^- \to e^+e^-\rho_L^0\ \rho_L^0$ are suppressed. Indeed, the final state of the process $e^+e^- \to \gamma\gamma\rho_L^0\ \rho_L^0$, with photons of the same energy deposit in detector as outgoing leptons, cannot be distinguished with the final state of $e^+e^- \to e^+e^-\rho_L^0\rho_L^0$.

We shall argue that the process $e^+e^- \to \gamma\gamma\rho_L^0\ \rho_L^0$ leads to a cross-section which is negligible at ILC. Let us first start with the process $e^+e^- \to \rho_L^0\rho_L^0$ illustrated in Fig.14(a), studied in Ref.[21, 22].

Its differential cross-section behaves typically like

$$\frac{d\sigma}{dt} \propto \frac{\alpha_{em}^4 f_\rho^4}{s^2 m_\rho^4}\,, \tag{5.6}$$

with the virtualities of the photons propagators equal to m_ρ^2. More accurate expressions can be found in [22], if one identifies $g_{V\gamma} = f_\rho\, m_\rho$.

Now, when considering the competitor process $e^+e^- \to \gamma\gamma\rho_L^0\ \rho_L^0$, that is adding two additional bremsstrahlung photon as in Fig.14(b), we get

$$\frac{d\sigma^{\,e^+e^-\to\gamma\gamma\rho_L\rho_L}}{dt\,dy_1\,dy_2\,dQ_1^2\,dQ_2^2} \Big/ \frac{d\sigma^{\,e^+e^-\to e^+e^-\rho_L\rho_L}}{dt\,dy_1\,dy_2\,dQ_1^2\,dQ_2^2} \simeq \frac{\alpha_{em}^2 Q_1^4 Q_2^4}{\alpha_s^4 s^2 m_\rho^4} \tag{5.7}$$

which is suppressed at ILC energies, and would be of comparable order of magnitude only for colliders with cm energy of the order of a few GeV.

5.3 Results for cross-section

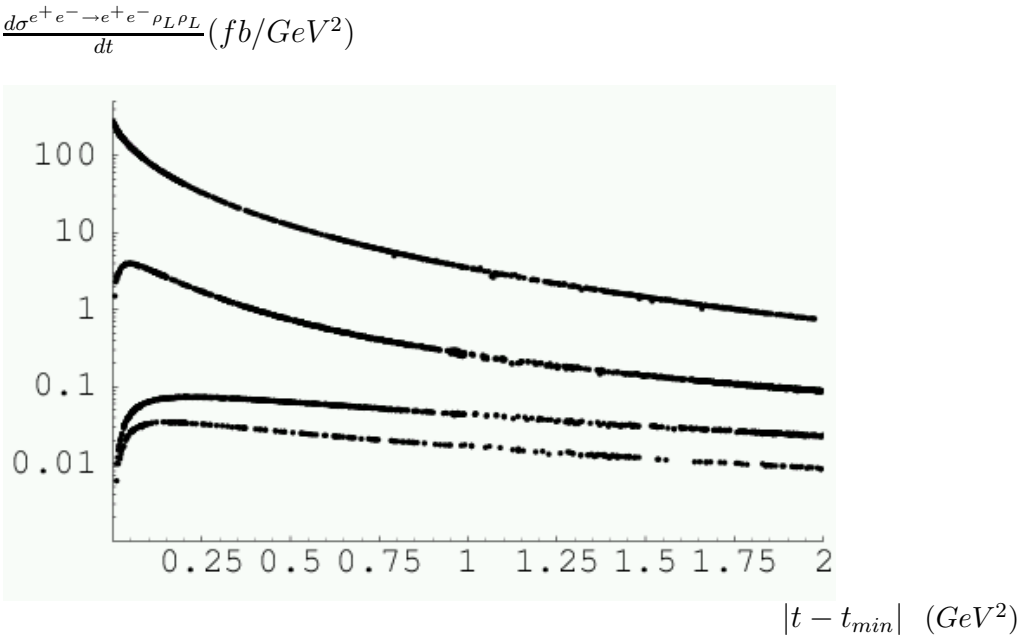

Figure 15: Cross-sections for $e^+e^- \to e^+e^-\rho_L^0\ \rho_L^0$ process. Starting from above, we display the cross-sections corresponding to the $\gamma_L^*\gamma_L^*$ mode, to the $\gamma_L^*\gamma_T^*$ modes, to the $\gamma_T^*\gamma_{T'}^*$ modes with different $T \neq T'$ and finally to the $\gamma_T^*\gamma_{T'}^*$ modes with the same $T = T'$.

We now display in Fig.15 the cross-sections $\frac{d\sigma^{e^+e^-\to e^+e^-\rho_L\rho_L}}{dt}$ as a function of t for the different polarizations, which are plotted after integrating the differential cross-section in (5.1) over the phase space considered previously. We made the following assumptions: we choose the QCD coupling constant to be $\alpha_s(\sqrt{Q_1Q_2})$ running at three loops, the parameter $c = 1$ which enters in the Regge limit condition and the cm energy $\sqrt{s} = 500$ GeV. Fig.15 shows for e^+e^- scattering the same differential cross-sections related to different photon helicities as Fig.5. We see that the shapes of corresponding curves are similar although they lead to quite different values of cross-sections. The cross-sections corresponding to photons with at least one transverse polarization vanish as in the $\gamma^*\gamma^*$ (cf subsection 4.2)

case at $t = t_{min}$. Similarly, each of them has a maximum in the very small t region. These maxima are shown more accurately on the log-log plot in Fig.16.

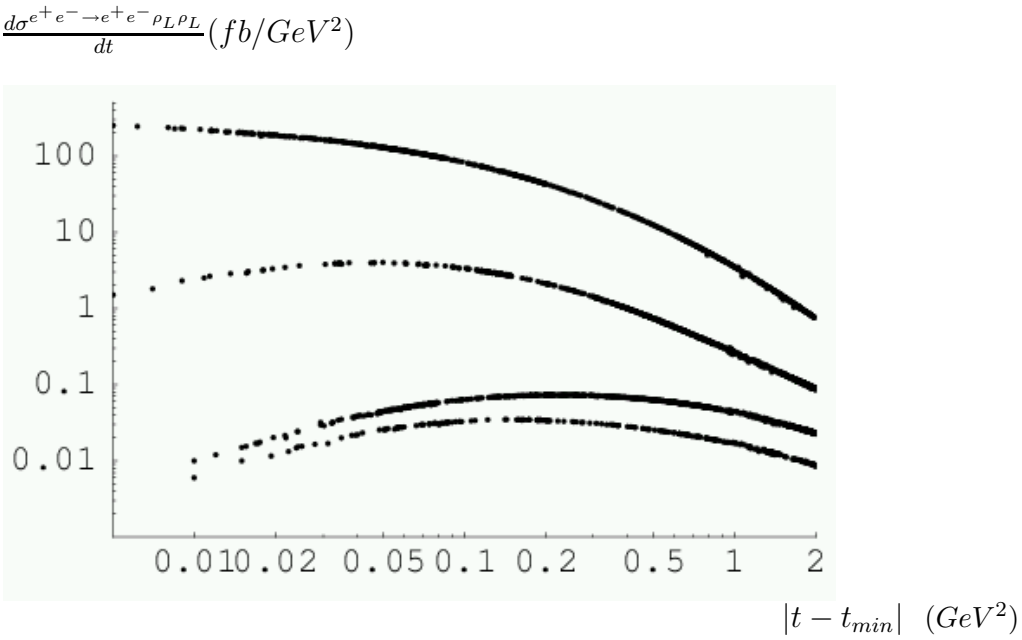

Figure 16: Cross-sections for $e^+e^- \to e^+e^-\rho_L^0\,\rho_L^0$ process, in log-log scale. Starting from above, we display the cross-sections corresponding to the $\gamma_L^*\gamma_L^*$ mode, to the $\gamma_L^*\gamma_T^*$ modes, to the $\gamma_T^*\gamma_{T'}^*$ modes with different $T \neq T'$ and finally to the $\gamma_T^*\gamma_{T'}^*$ modes with the same $T = T'$.

At this point one technical remark is in order. By looking into the upper plot in Fig.16 related to the $\mathcal{M}_{00}$ amplitude, one sees that the points corresponding to nonzero $|t-t_{min}|$ approach smoothly the point on the axis $|t-t_{min}| = 0$. This point $|t-t_{min}| = 0$ is of special interest because it gives the maximum of the total cross-section (since the transverse polarization case vanishes at t_{min}) and then practically dictates the trend of the total cross-section which is strongly peaked in the forward direction (for the longitudinal case) and strongly decreases with t (for all polarizations), as shown already at the level of the $\gamma^*\gamma^*$ cross-sections in subsection 4.2. Due to numerical instabilities, the differential cross-section at $|t-t_{min}| = 0$ must be evaluated in a different way than those for $|t-t_{min}| \neq 0$, i.e. by the use of expression (4.10) in which the integration over z_i was already done in the analytic way. Since Eq.(4.10) involves several polylogarithmic functions its structure of cuts is quite inconvenient for further numerical integration over variables y_i and Q_i. In order to overcome this technical problem it is useful to rewrite (4.10) by the use of Euler identity [23] in the form

$$\mathcal{M}_{00} = -is\,\frac{N_c^2-1}{N_c^2}\,\alpha_s^2\,\alpha_{em}\,f_\rho^2\,\frac{9\pi^2}{2}\,\frac{1}{Q_1^2Q_2^2}\left[6\left(R+\frac{1}{R}\right)\ln^2 R\right. \tag{5.8}$$
$$+12\left(R-\frac{1}{R}\right)\ln R\,+\,12\left(R+\frac{1}{R}\right)\,+\left(3\,R^2+\,2\,+\frac{3}{R^2}\right)\left(\left(\frac{\pi^2}{6}-\mathrm{Li}_2\,(1-R)\right)\ln R\right.$$
$$\left.\left.-\ln\,(R+1)\,\ln^2 R\,-\,2\,\mathrm{Li}_2\,(-R)\,\ln R\,+\,\mathrm{Li}_2\,(R)\,\ln R\,+\,2\,\mathrm{Li}_3\,(-R)\,-\,2\,\mathrm{Li}_3\,(R)\right)\right]\,.$$

since now the imaginary terms only come from $\mathrm{Li}_2(R)$ and $\mathrm{Li}_3(R)$ along their cuts, which cancels among each other analytically. Therefore, one can safely use their real part in a numerical fortran code as defined in standard packages.

The ILC collider is expected to run at a cm nominal energy of 500 GeV, though it might be extended in order to cover a range between 200 GeV and 1 TeV. Because of this possibility, we below discuss how the change of the energy in cms influences our predictions for the cross-sections measured in the same BeamCal detector. Furthermore, we discuss the effects of our various assumptions on the cross-section $\frac{d\sigma^{e^+e^-\to e^+e^-\rho_L\rho_L}}{dt}$ at the point t_{min}, and consequently on the behaviour of the total cross-section.

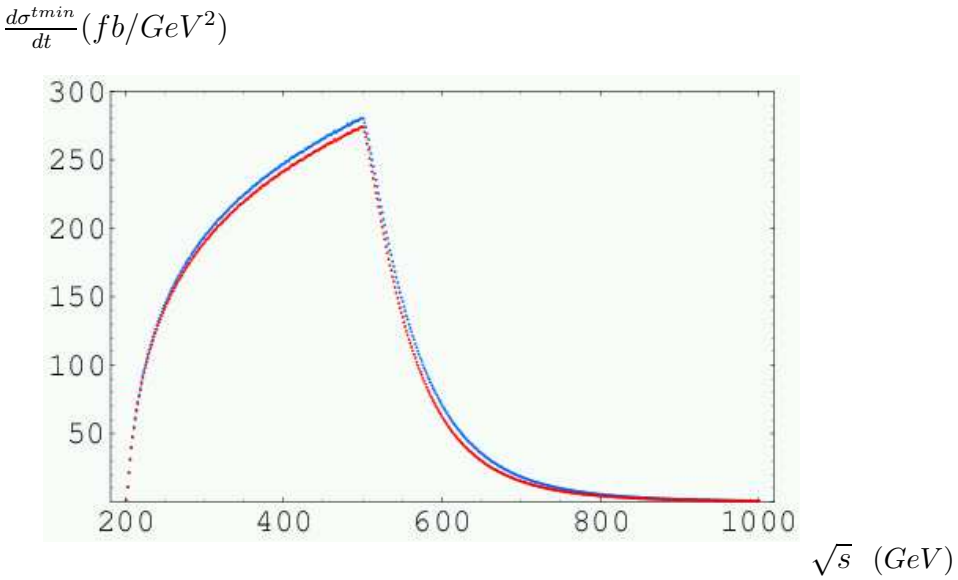

Figure 17: Cross-sections for $e^+e^- \to e^+e^-\rho_L^0\,\rho_L^0$ at $t = t_{min}$ for different α_s : the blue and red curves for α_s running respectively at one and three loops, with $c = 1$.

Fig.17 shows the cross-section at t_{min} as a function of the cm energy $\sqrt{s}$ for different choices of strong coupling constant α_s. To see the sensitivity of our predictions to these choices, we plot the cross-section at t_{min} in two cases: the blue curve corresponds to $\alpha_s(\sqrt{Q_1Q_2})$ running at one loop and the red one to $\alpha_s(\sqrt{Q_1Q_2})$ running at three loops. The curves in Fig.17 are very close to each other, which leads to a small uncertainty on the total cross-section as we will see in the following.

The shapes of plots in Fig.17 distinguish two different domains: if the planned cm energy range $\sqrt{s}$ is lower than 500 GeV, the function $f(Q_i)$ (cf. equation (5.3)) appearing as a constraint on the minimum value of y_i in the phase space integration domain does not play any role at $\theta_{min} = 4$ mrad. Thus the cross-section increases with $\sqrt{s}$ between 200 and 500 GeV. Because of the condition we assumed on the minimal value of the energies of the scattered leptons in the section 5.1, the y_i integration domain becomes very narrow (cf. equation (5.4)) when $\sqrt{s}$ goes to 200 GeV and leads to a strong decreasing of the cross-section at this cm energy. Note that if $\sqrt{s}$ becomes bigger than 500 GeV, $f(Q_i)$ will cut the small y_i region (which contribute mainly because of the Weizsäcker-Williams

photons fluxes) when $\sqrt{s}$ increases. Thus the cross-section falls down between 500 GeV and 1 TeV. This is due to the limitation caused by the minimal detection angle offered by the BeamCal calorimeter, which is thus optimal for our process when $\sqrt{s} = 500$ GeV. This effect on $f(Q_i)$ could be compensated if one could increase the value of Q_i but this would be completely suppressed because of the strong decreasing of the amplitude with Q_i. The above discussion leads also to the conclusion, that although the Born order cross-sections do not depend on s, the triggering effects introduce an s-dependence of the measured cross-sections.

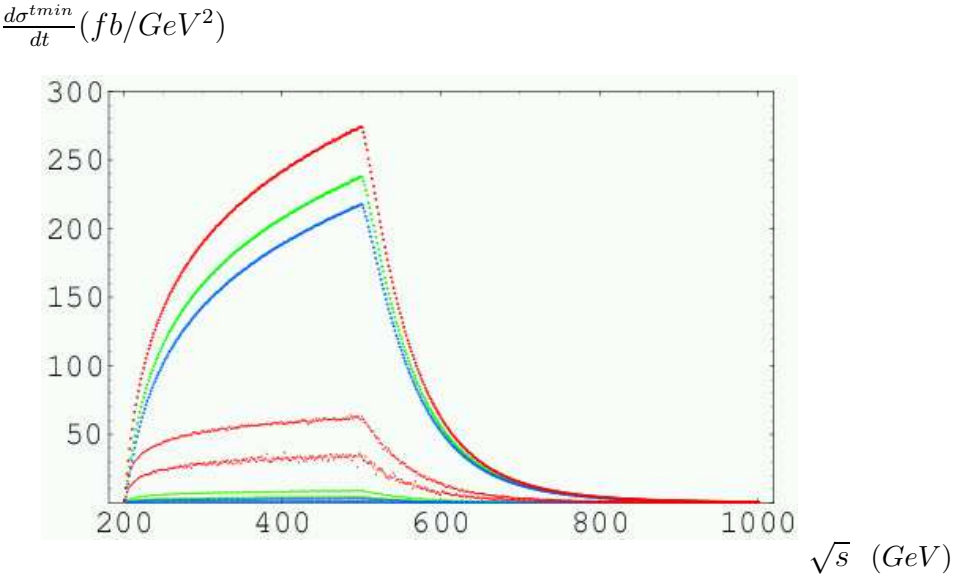

Figure 18: Cross-sections for $e^+e^- \to e^+e^-\rho_L^0\ \rho_L^0$ at $t = t_{min}$ for different values of the parameter c: the red curves correspond to $c = 1$, the green curves to $c = 2$ and and the blue curves to $c = 3$. For each value of c, by decreasing order the curves correspond to gluon-exchange, quark-exchange with longitudinal virtual photons and quark-exchange with transverse virtual photons.

Fig.18 shows the cross-section at t_{min} for different values of the parameter c which enters in the Regge limit condition $s_{\gamma^*\gamma^*} = y_1\, y_2\, s > c\, Q_1\, Q_2$. The value of the parameter c controls the dominance of gluonic contributions to the scattering amplitude: the increase of c should lead to suppression of quark exchanges. To see that we display the quark contribution in the same bins: we use the usual phase-space for the process $e^+e^- \to e^+e^-\rho_L^0\ \rho_L^0$ (cf. Eq.(2.2)) with the expressions of the amplitudes (4.15) and (4.16), and perform their numerical integration on y_i, Q_i with the same cuts as in the two gluon exchange process (cf. section 5.1). For each value of c we plot the three curves corresponding to the two gluon exchange process and the quark exchange processes with longitudinal and transverse virtual photons.

A technical remark is in order when performing this integration numerically. The equation (4.16) is not divergent when $Q_i^2 \to s$ because this limit is only valid if $s(1 - Q_1^2/s)(1 - Q_2^2/s)$ is finite and positive since this term corresponds in our notation to the cm energy of the virtual photons. In order to avoid numerical instabilities we add the condition $y_1 y_2 s > Q_1^2, Q_2^2$ to the Regge limit condition. We can check that this

supplementary constraint does not change our results for the other contributions, namely for the two gluon exchange and the quark exchange with longitudinal virtual photons processes.

As expected, the quark contribution is suppressed when increasing c and becomes completely negligible as soon as c exceeds 2. All above discussion concerned the case $t = t_{min}$ which determines the general trend of the cross-section in the non forward case. Because of that we hope that above conclusions are also valid at the level of the integrated over t cross-section. Thus, we omit bellow the quark exchanges.

We finally obtain the following results for the total cross-section integrated over t. We shall show three different predictions which differ by the choice of the definition of the coupling constant and by the choice of the value of the parameter c controlling the gluon dominance. First we choose $\alpha_s(\sqrt{Q_1Q_2})$ running at three loops, the constant $c = 1$, the cm energy $\sqrt{s} = 500$ GeV and we obtain (up to numerical uncertainties):

$$\begin{aligned} \sigma^{LL} &= 32.4\, fb \\ \sigma^{LT} &= 1.5\, fb \\ \sigma^{TT} &= 0.2\, fb \end{aligned} \tag{5.9}$$

and then

$$\sigma^{Total} = 34.1\, fb. \tag{5.10}$$

With a nominal integrated luminosity of $125\,\mathrm{fb}^{-1}$, this will yield $4.26\,10^3$ events per year.

Secondly, with the choice of $\alpha_s(\sqrt{Q_1Q_2})$ running at one loop, the constant $c = 1$ and the cm energy $\sqrt{s} = 500$GeV, we obtain:

$$\begin{aligned} \sigma^{LL} &= 33.9\, fb \\ \sigma^{LT} &= 1.5\, fb \\ \sigma^{TT} &= 0.2\, fb \end{aligned} \tag{5.11}$$

which leads to

$$\sigma^{Total} = 35.6\, fb. \tag{5.12}$$

As expected, we see that the transition from three to one loop changes very little the total cross-section. This result will yield $4.45\,10^3$ events per year with a nominal integrated luminosity of $125\,\mathrm{fb}^{-1}$.

In the third choice, we choose $\alpha_s(\sqrt{Q_1Q_2})$ running at three loops, the same cm energy $\sqrt{s} = 500$GeV and the constant $c = 2$ (for which as previously discussed quark exchanges are completely negligible) and we get:

$$\begin{aligned} \sigma^{LL} &= 28.1\, fb \\ \sigma^{LT} &= 1.3\, fb \\ \sigma^{TT} &= 0.2\, fb \end{aligned} \tag{5.13}$$

which imply

$$\sigma^{Total} = 29.6\, fb. \tag{5.14}$$

This result will yield $3.7\,10^3$ events per year with a nominal integrated luminosity of $125\,\mathrm{fb}^{-1}$.

All the prediction above were obtained using the asymptotical DA. In order to see the sensitivity of this assumption on our results, we do also the calculation using the DA (4.9) within different models. The choice of the DA of Ref.[24] with $a_2 = -0.1$ and $a_4 = 0$ gives $4.2\,10^3$ events per year, while the choice of the DA of Ref.[25] with $a_2 = 0.05$ and $a_4 = 0$ gives $4.3\,10^3$ events per year.

In summary of this part we see that our predictions are quite stable when changing the main parameters characterizing the theoretical uncertainties of our approach.

The obvious question which appears now is how our predictions summarized by Eqs. (5.10-5.14) will change by the inclusion of the BFKL resummation effects. Generaly BFKL evolution increases value of cross-sections, which means that the results obtained at Born approximation can be considered as a lower limit of cross-sections for ρ-mesons pairs production with complete BFKL evolution taken into account. Although the complete analysis of BFKL evolution for our process is beyond the scope of the present paper, we would like to finish this section with a few remarks on possible effects caused by the BFKL evolution. We consider below only the point $t = t_{min}$ and we restrict ourselves to the leading order BFKL evolution[4]. In the Fig.19 we show the corresponding cross-section

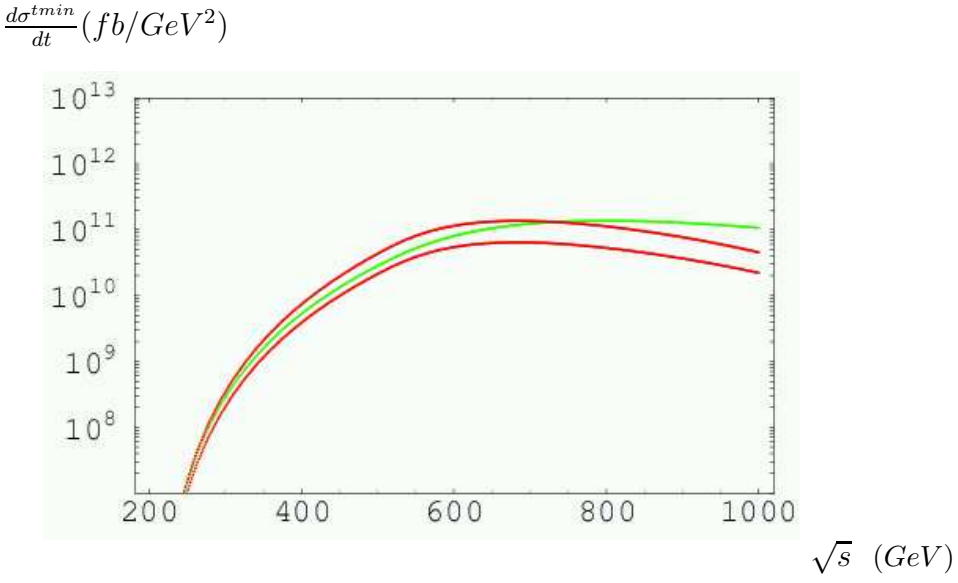

Figure 19: Cross-sections for $e^+e^- \to e^+e^-\rho_L^0\ \rho_L^0$ with LO BFKL evolution at $t = t_{min}$ for different α_s : the upper and lower red curves for α_s running respectively at one and three loops and the green one for $\alpha_s = 0.46$.

at t_{min} as a function of $\sqrt{s}$, for different choices of α_s: we considered α_s running at one

[4]Note that related studies with a hard scale provided by t and not by Q^2 were performed in [26]

and three loops (red curves) as in the previous discussion for the two gluon exchange and we also used a fixed value of α_s (green curve) corresponding to the three loops running coupling constant at a typical virtuality $Q = 1.1$ GeV. We have used the expression of the BFKL amplitude [8] for the forward case in the saddle point approximation, namely

$$A(s, t = t_{min}, Q_1, Q_2) \sim is\,\pi^5\sqrt{\pi}\,\frac{9(N_c^2-1)}{4N_c^2}\,\frac{\alpha_s^2\alpha_{em}f_\rho^2}{Q_1^2Q_2^2}\,\frac{e^{4\ln 2\,\bar{\alpha}_s Y}}{\sqrt{14\bar{\alpha}_s\zeta(3)Y}}\exp\left(-\frac{\ln^2 R}{14\bar{\alpha}_s\zeta(3)Y}\right), \tag{5.15}$$

with the rapidity $Y = \ln(\frac{c'\,s\,y_1\,y_2}{Q_1Q_2})$, $\bar{\alpha}_s = \frac{N_c}{\pi}\alpha_s(\sqrt{Q_1Q_2})$ and $R = \frac{Q_1}{Q_2}$. The plots in Fig.19 are obtained by assuming that the constant c' in Eq.(5.15), which at LO is arbitrary and of order 1, is chosen to be 1. The factor $\exp(4\ln 2\,\bar{\alpha}_s Y)$ explains the enhancement of the sensitivity to the choice of α_s compared to the one in the Born two gluon exchange case, since $4\ln 2\ Y$ takes big values for ILC rapidities Y. For the same reasons as discussed earlier in this section, the function $f(Q_i)$ does not appear for $\sqrt{s}$ lower than 500 GeV; the LO BFKL cross-section then grows exponentially with s in this domain. The effect of $f(Q)$ starting from 500 GeV gives an inflexion point of the curves and a maximum beyond 500 GeV; then the curves decrease until 1TeV.

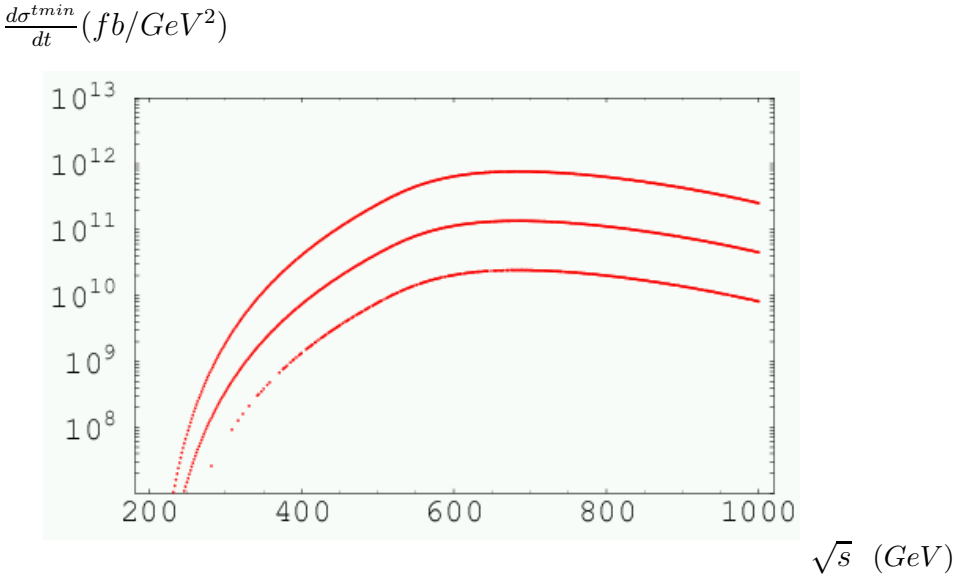

Figure 20: LO BFKL cross-section for $e^+e^- \to e^+e^-\rho_L^0\,\rho_L^0$ at $t = t_{min}$ for different values of the parameter c': by decreasing order, the curves correspond to $c' = 2$, $c' = 1$ and $c' = 0.5$. c is fixed to be equal to 1.

The effect of varying the parameter c' in the BFKL prediction is illustrated in Fig.20. As expected, it has a strong effect in the order of magnitude of the differential cross-section, since the rapidity is very high and thus leads to a large value of the factor $\exp(4\ln 2\,\bar{\alpha}_s Y)$, which is highly sensitive to the precise definition of the rapidity.

Obviously the order of magnitude of the LO BFKL cross-section will be suppressed at NLO, which is presumably more realistic. From previous studies at the level of $\gamma^*\gamma^*$ [8],[15], the NLO contribution is expected to be between LO and Born order cross-section.

This is to be preserved at the level of the e^+e^- process. The comparison of Figs.17-18 with Figs.19-20 leads to the conclusions that the BFKL evolution changes the shape of the cross-section: when increasing $\sqrt{s}$ from 500 GeV to 1 TeV, the two gluon exchange cross-section will fall down, while with the BFKL resummation effects, the cross-section should more or less stay stable, with a high number of events to be still observed for these cm energies.

6 Conclusion

The present study should be considered as a continuation of our previous investigations [6],[7],[8] for the production of two ρ_L^0-mesons in the scattering of two longitudinally polarized virtual photons. The diffractive production of a meson pair is one of the gold plated processes which permit clean studies of the BFKL dynamics at ILC. Our main motivation in the present work was to estimate, in the Born approximation, the cross-section for production of ρ_L^0-meson pairs in the e^+e^- collisions occurring in the kinematical conditions of future ILC. For this aim, we first calculated contributions, missing up to now, which involve the helicity amplitudes with transversally polarized virtual photons. This was done in a mostly analytic way, by the use of techniques developped in Ref.[7]. Having done, we calculated the cross-section for the electroproduction of ρ_L^0-meson pairs which takes into account kinematical cuts imposed by the LDC design project for the BeamCal detector. By assuming a nominal value of the integrated luminocity, we predict (in the numerical analysis of cross-sections) a production of at least $4\ 10^3$ meson pairs per year, a value which is sufficiently large to ensure a reliable data analysis.

We discussed a possible background process in the BeamCal detector which can identify in a misleading way an outgoing lepton with a photon. We predict that the cross-section for such a background process is negligibly small at ILC energies.

Finally we discussed theoretical uncertainties of obtained estimates. There are two main sources of them. The first one is related to the assumptions we have made to characterize the Regge limit and the particular role played by the parameter c; we also observe a sensitivity of our results on the choice of the running coupling constant.

The second source of theoretical uncertainties of our estimates is related to taking into account effects of the BFKL evolution. Generally, an inclusion of the BFKL evolution increases significantly the cross-section, as one sees from comparison of Fig.17 with Fig.19 obtained within the LO BFKL approach. On the other hand it is known that this increase of predictions for cross-sections is smaller if the BFKL evolution is considered at the next-to-leading order. Because of that we can safely say that our predictions should be considered as a lower limit of predictions which are obtained by taking into account BFKL effects at NLO. We hope to consider this issue in our future publications.

In principle, the same techniques can be applied for the description of processes involving other final states, both with positive charge parity exchange in $t-$channel, e.g. J/Ψ pairs, as well as negative charge parity, e.g. $\gamma^*\gamma^* \to \eta_c\eta_c$ [27].

Acknowledgements:

We thank G. Korchemsky, S. Munier, B. Pire, R. Poeschl and F. Richard for many discussions and comments. This work is supported by the Polish Grant 1 P03B 028 28, the French-Polish scientific agreement Polonium. L.Sz. is a Visiting Fellow of the Fonds National pour la Recherche Scientifique (Belgium).

7 Appendix

In this appendix we collect the analytical expressions of the coefficients $a(\underline{r}; Q_1, Q_2; z_1, z_2)$, $b(\underline{r}; Q_1, Q_2; z_1, z_2)$ and $f(\underline{r}; Q_1, Q_2; z_1, z_2)$, as well as all the generic integrals which appear in the computation of the Born amplitude in section 4. The coefficients a, b and f can be expressed as combinations of several generic integrals

$$\begin{aligned} a(\underline{r}; Q_1, Q_2; z_1, z_2) &= \frac{1}{2}\left[I_{3\mu_1\mu_2}(z_1,\, z_2) + I_{3\mu_1\mu_2}(\bar{z}_1,\, \bar{z}_2) - I_{3\mu_1\mu_2}(\bar{z}_1,\, z_2) - I_{3\mu_1\mu_2}(z_1,\, \bar{z}_2)\right] \\ &\quad -\frac{r^2}{2}\left[I_{4\mu_1\mu_2}(z_1,\, z_2) - I_{4\mu_1\mu_2}(\bar{z}_1,\, z_2)\right] \\ &\quad -\frac{1}{r^2}\left[J^c_{\mu_1\mu_2}(z_1,\, \bar{z}_2) + J^c_{\mu_1\mu_2}(\bar{z}_1,\, z_2) - J^c_{\mu_1\mu_2}(\bar{z}_1,\, \bar{z}_2) - J^c_{\mu_1\mu_2}(z_1,\, z_2)\right], \end{aligned} \tag{7.1}$$

$$\begin{aligned} b(\underline{r}; Q_1, Q_2; z_1, z_2) &= \left[\frac{z_1 z_2}{(z_1^2\underline{r}^2+\mu_1^2)(z_2^2\underline{r}^2+\mu_2^2)} - \frac{z_1\bar{z}_2}{(z_1^2\underline{r}^2+\mu_1^2)(\bar{z}_2^2\underline{r}^2+\mu_2^2)}\right. \\ &\quad \left. - \frac{\bar{z}_1 z_2}{(\bar{z}_1^2\underline{r}^2+\mu_1^2)(z_2^2\underline{r}^2+\mu_2^2)} + \frac{\bar{z}_1\bar{z}_2}{(\bar{z}_1^2\underline{r}^2+\mu_1^2)(\bar{z}_2^2\underline{r}^2+\mu_2^2)}\right] r^2 I_2 \\ &\quad + \left(\left[\frac{z_1}{z_1^2\underline{r}^2+\mu_1^2} - \frac{\bar{z}_1}{\bar{z}_1^2\underline{r}^2+\mu_1^2}\right]\left[I_{2\mu_2}(\bar{z}_2) - I_{2\mu_2}(z_2) + r^2(\bar{z}_2 - z_2) I_{3\mu_2}(z_2)\right] + (1 \leftrightarrow 2)\right) \\ &\quad + r^2\left[\frac{1}{2} + 2z_1 z_2 - (z_1 + z_2)\right]\left[I_{4\mu_1\mu_2}(z_1,\, z_2) + I_{4\mu_1\mu_2}(z_1,\, \bar{z}_2)\right] \\ &\quad + \left[-\frac{1}{2} + (z_1 + z_2)\right] I_{3\mu_1\mu_2}(z_1,\, z_2) + \left[\frac{3}{2} - (z_1 + z_2)\right] I_{3\mu_1\mu_2}(\bar{z}_1,\, \bar{z}_2) \\ &\quad + \left[z_1 - z_2 - \frac{1}{2}\right] I_{3\mu_1\mu_2}(\bar{z}_1,\, z_2) + \left[z_2 - z_1 - \frac{1}{2}\right] I_{3\mu_1\mu_2}(z_1,\, \bar{z}_2)] \\ &\quad + \frac{1}{r^2}[J^c_{\mu_1\mu_2}(z_1,\, \bar{z}_2) + J^c_{\mu_1\mu_2}(\bar{z}_1,\, z_2) - J^c_{\mu_1\mu_2}(\bar{z}_1,\, \bar{z}_2) - J^c_{\mu_1\mu_2}(z_1,\, z_2)], \end{aligned} \tag{7.2}$$

$$\begin{aligned} f(\underline{r}; Q_1, Q_2; z_1, z_2) &= \left[\frac{1}{z_1^2\underline{r}^2+\mu_1^2} + \frac{1}{\bar{z}_1^2\underline{r}^2+\mu_1^2}\right]\left[\frac{z_2}{z_2^2\underline{r}^2+\mu_2^2} - \frac{\bar{z}_2}{\bar{z}_2^2\underline{r}^2+\mu_2^2}\right] I_2 \\ &\quad + 2\left[\frac{\bar{z}_2}{\bar{z}_2^2\underline{r}^2+\mu_2^2} - \frac{z_2}{z_2^2\underline{r}^2+\mu_2^2}\right] I_{3\mu_1}(z_1) + (\bar{z}_2 - z_2)\left[\frac{1}{z_1^2\underline{r}^2+\mu_1^2} + \frac{1}{\bar{z}_1^2\underline{r}^2+\mu_2^2}\right] I_{3\mu_2}(z_2) \\ &\quad + (z_2 - \bar{z}_2)\left[I_{4\mu_1\mu_2}(z_1, z_2) + I_{4\mu_1\mu_2}(\bar{z}_1, z_2)\right] + \frac{1}{r^2}\left[\frac{1}{z_1^2\underline{r}^2+\mu_1^2} + \frac{1}{\bar{z}_1^2\underline{r}^2+\mu_1^2}\right]\left[I_{2\mu_2}(\bar{z}_2) - I_{2\mu_2}(z_2)\right] \\ &\quad + \frac{1}{r^2}[I_{3\mu_1\mu_2}(\bar{z}_1,\, z_2) - I_{3\mu_1\mu_2}(z_1,\, \bar{z}_2) + I_{3\mu_1\mu_2}(z_1,\, z_2) - I_{3\mu_1\mu_2}(\bar{z}_1,\, \bar{z}_2)], \end{aligned} \tag{7.3}$$

part of which are divergent integrals

$$I_2 = \int \frac{d^d\underline{k}}{\underline{k}^2(\underline{k}-\underline{r})^2}\,, \tag{7.4}$$

$$I_{2m}(a) = \int \frac{d^d\underline{k}}{\underline{k}^2((\underline{k}-a\underline{r})^2+m^2)}\,, \tag{7.5}$$

$$I_{3m}(a) = \int \frac{d^d\underline{k}}{\underline{k}^2(\underline{k}-\underline{r})^2((\underline{k}-a\underline{r})^2+m^2)}\,, \tag{7.6}$$

$$I_{3m_am_b}(a,\,b) = \int \frac{d^d\underline{k}}{\underline{k}^2((\underline{k}-a\underline{r})^2+m_a^2)((\underline{k}-b\underline{r})^2+m_b^2)}\,, \tag{7.7}$$

$$I_{4m_am_b}(a,\,b) = \int \frac{d^d\underline{k}}{\underline{k}^2(\underline{k}-\underline{r})^2((\underline{k}-a\underline{r})^2+m_a^2)((\underline{k}-b\underline{r})^2+m_b^2)}\,, \tag{7.8}$$

and some of them are finite

$$J_{2m_am_b}(a,\,b) = \int \frac{d^d\underline{k}}{((\underline{k}-a\,\underline{r})^2+m_a^2)((\underline{k}-b\,\underline{r})^2+m_b^2)}\,, \tag{7.9}$$

$$J^c_{m_am_b}(a,\,b) = \int \frac{d^d\underline{k}\;(\underline{k}\cdot\underline{r})}{\underline{k}^2((\underline{k}-a\,\underline{r})^2+m_a^2)((\underline{k}-b\,\underline{r})^2+m_b^2)}\,, \tag{7.10}$$

$$K_{m_am_b}(a,\,b) = \int \frac{d^d\underline{k}}{\underline{k}^2}\left[\frac{1}{(b^2\underline{r}^2+m_b^2)[(\underline{k}-a\underline{r})^2+m_a^2]}+\frac{1}{(a^2\underline{r}^2+m_a^2)[(\underline{k}-b\underline{r})^2+m_b^2]}\right.$$
$$\left.-\frac{2r^2}{[\underline{k}^2+(\underline{r}-\underline{k})^2](a^2\underline{r}^2+m_a^2)(b^2\underline{r}^2+m_b^2)}\right]\,, \tag{7.11}$$

$$L_{m_am_b}(a,\,b) = \int \frac{d^d\underline{k}}{\underline{k}^2}\left[\frac{1}{(a^2\underline{r}^2+m_a^2)[(\underline{k}-b\underline{r})^2+m_b^2]}\right. \tag{7.12}$$
$$\left.-\frac{r^2}{[\underline{k}^2+(\underline{r}-\underline{k})^2](a^2\underline{r}^2+m_a^2)(b^2\underline{r}^2+m_b^2)}\right]\,,$$

$$N_{m_am_b}(a,\,b) = \int \frac{d^d\underline{k}}{\underline{k}^2}\left[\frac{1}{(a^2\underline{r}^2+m_a^2)[(\underline{k}-b\underline{r})^2+m_b^2]}-\frac{1}{(b^2\underline{r}^2+m_b^2)[(\underline{k}-a\underline{r})^2+m_a^2]}\right]\,, \tag{7.13}$$

$$J_{3\mu}(a) = \int \frac{d^2\underline{k}}{\underline{k}^2(\underline{k}-\underline{r})^2}\left[\frac{1}{(\underline{k}-\underline{r}a)^2+\mu^2}-\frac{1}{a^2\underline{r}^2+\mu^2}+(a\leftrightarrow\bar{a})\right]\,, \tag{7.14}$$

$$J_{4\mu_1\mu_2}(z_1,\,z_2) = \int \frac{d^2\underline{k}}{\underline{k}^2(\underline{k}-\underline{r})^2} \tag{7.15}$$
$$\times\left[\frac{1}{((\underline{k}-\underline{r}z_1)^2+\mu_1^2)((\underline{k}-\underline{r}z_2)^2+\mu_2^2)}-\frac{1}{(z_1^2\underline{r}^2+\mu_1^2)(z_2^2\underline{r}^2+\mu_2^2)}+(z\leftrightarrow\bar{z})\right]\,.$$

Although divergent integrals (7.4-7.8) enter formulas (7.1,7.2 and 7.3), the coefficients $a(\underline{r};Q_1,Q_2;z_1,z_2)$, $b(\underline{r};Q_1,Q_2;z_1,z_2)$ and $f(\underline{r};Q_1,Q_2;z_1,z_2)$ are finite expressions. This requires a tracing of the cancellation of divergencies within each of these coefficients which in principle can be done within a dimensional regularization scheme. Unfortunately this

procedure is not always practically feasible, especially for the integrals I_{3m}, $I_{3m_1m_2}$ or $I_{4m_1m_2}$, which apart of massless propagators contain also massive propagators. These integrals can be rewritten in terms of simpler, although divergent integrals I_2 and I_{2m} as

$$\begin{aligned} I_{3m_1m_2}(z_1,\,z_2) &= -\frac{1}{2}\left(\frac{1}{z_1^2\underline{r}^2+m_1^2}+\frac{1}{z_2^2\underline{r}^2+m_2^2}\right)J_{2m_1m_2}(z_1,\,z_2) \qquad (7.16)\\ &+\left(\frac{z_1}{z_1^2\underline{r}^2+m_1^2}+\frac{z_2}{z_2^2\underline{r}^2+m_2^2}\right)J^c_{m_1m_2}(z_1,\,z_2)+\frac{1}{2(z_2^2\underline{r}^2+m_2^2)}I_{2m_1}(z_1)+\frac{1}{2(z_1^2\underline{r}^2+m_1^2)}I_{2m_2}(z_2)\,,\\ I_{4m_1m_2}(z_1,\,z_2) &= \frac{1}{2}\left(\frac{1}{(z_1^2\underline{r}^2+m_1^2)(z_2^2\underline{r}^2+m_2^2)}+\frac{1}{(\bar{z}_1^2\underline{r}^2+m_1^2)(\bar{z}_2^2\underline{r}^2+m_2^2)}\right)I_2\\ &\quad+\frac{1}{2}J_{4m_1m_2}(z_1,\,z_2)\,, \qquad (7.17)\\ I_{3_m}(z) &= \frac{1}{2}\left(\frac{1}{z^2\underline{r}^2+m^2}+\frac{1}{\bar{z}^2\underline{r}^2+m^2}\right)I_2+\frac{1}{2}J_{3m}(z)\,. \qquad (7.18)\end{aligned}$$

Divergent integrals like I_2 and I_{2m} or finite ones like $J^c_{m_1m_2}$ and $J_{2m_1m_2}$ are directly computed by standard Feynman techniques.

The finite integrals $J_{4m_1m_2}$ and J_{3m} are calculated by the use of the change of variables defined by the inverse conformal transformation applied to the momenta and other dimensional parameters of integrals, see [5] for details. Such a change of variables applied to the two-dimensional, UV and IR finite integrals results in a reduction of number of massless propagators, a well known property from the studies of conformal field theories in coordinate space [28].

As a result, we get the following expressions for the coeffcients $a(\underline{r};Q_1,Q_2;z_1,z_2)$, $b(\underline{r};Q_1,Q_2;z_1,z_2)$ and $f(\underline{r};Q_1,Q_2;z_1,z_2)$ which involve only explicitely convergent integrals

$$\begin{aligned} a(\underline{r},z_1,\,z_2) &= \qquad (7.19)\\ &\left(\frac{1}{2}\left[\frac{z_1}{(z_1^2\underline{r}^2+\mu_1^2)}+\frac{z_2}{(z_2^2\underline{r}^2+\mu_2^2)}+\frac{1}{r^2}\right]J^c_{\mu_1\mu_2}(z_1,\,z_2)+\frac{1}{4}K(z_1,\,z_2)\right.\\ &+(z_1\leftrightarrow\bar{z}_1,\,z_2\leftrightarrow\bar{z}_2)-(z_1\leftrightarrow\bar{z}_1)-(z_2\leftrightarrow\bar{z}_2))\\ &+\frac{r^2}{4}\left[J_{4\mu_1\mu_2}(\bar{z}_1,\,z_2)-J_{4\mu_1\mu_2}(z_1,\,z_2)\right]+\frac{1}{4}\left[\frac{1}{(z_1^2\underline{r}^2+\mu_1^2)}+\frac{1}{(z_2^2\underline{r}^2+\mu_2^2)}+\frac{1}{(\bar{z}_1^2\underline{r}^2+\mu_1^2)}\right.\\ &\left.+\frac{1}{(\bar{z}_2^2\underline{r}^2+\mu_2^2)}\right]\left[J_{2\mu_1\mu_2}(\bar{z}_1,\,z_2)-J_{2\mu_1\mu_2}(z_1,\,z_2)\right], \end{aligned}$$

$$\begin{aligned} b(\underline{r},z_1,\,z_2) &= \qquad (7.20)\\ &\frac{r^2}{2}\left[\frac{z_1}{z_1^2\underline{r}^2+\mu_1^2}-\frac{\bar{z}_1}{\bar{z}_1^2\underline{r}^2+\mu_1^2}\right][\bar{z}_2-z_2]\,J_{3\mu_2}(z_2)+(1\leftrightarrow 2)\\ &+r^2\left[\frac{1}{2}+2z_1z_2-(z_1+z_2)\right][J_{4\mu_1\mu_2}(z_1,\,z_2)+J_{4\mu_1\mu_2}(z_1,\,\bar{z}_2)]+\left[-\frac{1}{2}+z_1+z_2\right]\left[\left(\frac{z_1}{z_1^2\underline{r}^2+\mu_1^2}\right.\right. \end{aligned}$$

$$+\frac{z_2}{z_2^2\underline{r}^2+\mu_2^2}\Big)J^c_{\mu_1\mu_2}(z_1,\,z_2)-\frac{1}{2}\left(\frac{1}{z_1^2\underline{r}^2+\mu_1^2}+\frac{1}{z_2^2\underline{r}^2+\mu_2^2}\right)J_{2\mu_1\mu_2}(z_1,\,z_2)\Big]+\left[\frac{3}{2}-(z_1+z_2)\right]$$
$$\times\left[\left(\frac{\bar{z}_1}{\bar{z}_1^2\underline{r}^2+\mu_1^2}+\frac{\bar{z}_2}{\bar{z}_2^2\underline{r}^2+\mu_2^2}\right)J^c_{\mu_1\mu_2}(\bar{z}_1,\,\bar{z}_2)-\frac{1}{2}\left(\frac{1}{\bar{z}_1^2\underline{r}^2+\mu_1^2}+\frac{1}{\bar{z}_2^2\underline{r}^2+\mu_2^2}\right)J_{2\mu_1\mu_2}(\bar{z}_1,\,\bar{z}_2)\right]$$
$$+\left[z_1-z_2-\frac{1}{2}\right]\left[\left(\frac{\bar{z}_1}{\bar{z}_1^2\underline{r}^2+\mu_1^2}+\frac{z_2}{z_2^2\underline{r}^2+\mu_2^2}\right)J^c_{\mu_1\mu_2}(\bar{z}_1,\,z_2)-\frac{1}{2}\left(\frac{1}{\bar{z}_1^2\underline{r}^2+\mu_1^2}+\frac{1}{z_2^2\underline{r}^2+\mu_2^2}\right)\right.$$
$$\left.\times J_{2\mu_1\mu_2}(\bar{z}_1,\,z_2)\right]+\left[z_2-z_1-\frac{1}{2}\right]\left[\left(\frac{z_1}{z_1^2\underline{r}^2+\mu_1^2}+\frac{\bar{z}_2}{\bar{z}_2^2\underline{r}^2+\mu_2^2}\right)J^c_{\mu_1\mu_2}(z_1,\,\bar{z}_2)-\frac{1}{2}\left(\frac{1}{z_1^2\underline{r}^2+\mu_1^2}\right.\right.$$
$$\left.\left.+\frac{1}{\bar{z}_2^2\underline{r}^2+\mu_2^2}\right)J_{2\mu_1\mu_2}(z_1,\,\bar{z}_2)\right]+\frac{1}{r^2}\left[J^c_{\mu_1\mu_2}(z_1,\,\bar{z}_2)+J^c_{\mu_1\mu_2}(\bar{z}_1,\,z_2)-J^c_{\mu_1\mu_2}(\bar{z}_1,\,\bar{z}_2)\right.$$
$$\left.-J^c_{\mu_1\mu_2}(z_1,\,z_2)\right]+L_{\mu_1\mu_2}(\bar{z}_1,\,z_2)+L_{\mu_1\mu_2}(\bar{z}_2,\,z_1)-\frac{1}{4}[K_{\mu_1\mu_2}(z_1,\,z_2)+K(\bar{z}_1,\,\bar{z}_2)$$
$$+K_{\mu_1\mu_2}(z_1,\,\bar{z}_2)+K_{\mu_1\mu_2}(\bar{z}_1,\,z_2)]+\frac{z_2-z_1}{2}[N_{\mu_1\mu_2}(z_1,\,z_2)+N_{\mu_1\mu_2}(\bar{z}_2,\,\bar{z}_1)]$$
$$+\frac{z_1+z_2}{2}[N_{\mu_1\mu_2}(z_1,\,\bar{z}_2)+N_{\mu_1\mu_2}(z_2,\,\bar{z}_1)]\,,$$

$$f(\underline{r},z_1,\,z_2) = \left[\frac{\bar{z}_2}{\bar{z}_2^2\underline{r}^2+\mu_2^2}-\frac{z_2}{z_2^2\underline{r}^2+\mu_2^2}\right]J_{3\mu_1}(z_1) \tag{7.21}$$
$$+\frac{z_2-\bar{z}_2}{2}\left[J_{4\mu_1\mu_2}(z_1,\,z_2)+J_{4\mu_1\mu_2}(\bar{z}_1,\,z_2)-(\frac{1}{z_1^2\underline{r}^2+\mu_1^2}+\frac{1}{\bar{z}_1^2\underline{r}^2+\mu_1^2})J_{3\mu_2}(z_2)\right]$$
$$+\left(\frac{1}{r^2}\left[-\frac{1}{2}(\frac{1}{z_1^2\underline{r}^2+\mu_1^2}+\frac{1}{z_2^2\underline{r}^2+\mu_2^2})J_{2\mu_1\mu_2}(z_1,\,z_2)+(\frac{z_1}{z_1^2\underline{r}^2+\mu_1^2}\right.\right.$$
$$\left.\left.+\frac{z_2}{z_2^2\underline{r}^2+\mu_2^2})J^c_{\mu_1\mu_2}(z_1,\,z_2)\right]-(z_1\leftrightarrow\bar{z}_1,\,z_2\leftrightarrow\bar{z}_2)+(z_1\leftrightarrow\bar{z}_1)-(z_2\leftrightarrow\bar{z}_2)\right)$$
$$+\frac{1}{2r^2}\left[N(\bar{z}_1,\,\bar{z}_2)-N(z_1,\,z_2)+N(z_1,\,\bar{z}_2)-N(\bar{z}_1,\,z_2)\right]\,.$$

The separation of divergent and finite parts in all integrals involved was done within the dimensional regularization with $d=2+2\epsilon$. Thus for the simplest integral I_{2m} the result reads

$$I_{2m}(a)=\frac{\pi}{\epsilon(a^2\underline{r}^2+m^2)}(1+\epsilon(\ln\pi-\Psi(1)-\ln m^2+2\ln(a^2\underline{r}^2+m^2)))\,. \tag{7.22}$$

or for its massless case

$$I_2=\frac{2\pi}{\underline{r}^2\epsilon}(1+\epsilon(\ln(\pi\underline{r}^2)-\Psi(1)))\,. \tag{7.23}$$

We will use the finite part of I_2 and I_{2m} to compute the integrals in which they are involved. For example we can write the finite integrals $K_{m_am_b}$, $L_{m_am_b}$ and $M_{m_am_b}$ in term of the finite part of these integrals since the divergent parts ultimately cancel when we express them like

$$K_{m_1m_2}(z_1,\,z_2) = \frac{1}{z_2^2\underline{r}^2+m_2^2}I_{2m_1}(z_1)+\frac{1}{z_1^2\underline{r}^2+m_1^2}I_{2m_2}(z_2)$$

$$-\frac{r^2}{(z_1^2\underline{r}^2+m_1^2)(z_2^2\underline{r}^2+m_2^2)}I_2\,, \tag{7.24}$$

$$L_{m_1m_2}(z_1,\,z_2) = \frac{1}{z_1^2\underline{r}^2+m_1^2}I_{2m_2}(z_2)-\frac{r^2}{2(z_1^2\underline{r}^2+m_1^2)(z_2^2\underline{r}^2+m_2^2)}I_2\,, \tag{7.25}$$

$$N_{m_1m_2}(z_1,\,z_2) = \frac{1}{z_1^2\underline{r}^2+m_1^2}I_{2m_2}(z_2)-\frac{1}{z_2^2\underline{r}^2+m_2^2}I_{2m_1}(z_1)\,. \tag{7.26}$$

The integrals which involve only two massive propagators are finite and are calculated in a standard way using Feynman parameters. We obtain

$$\begin{aligned} J_{2m_am_b} &= \int\frac{d^d\underline{k}}{((\underline{k}-\underline{r}a)^2+m_a^2)((\underline{k}-\underline{r}b)^2+m_b^2)} \\ &= \frac{\pi}{\sqrt{\lambda}}\ln\frac{r^2(a-b)^2+m_a^2+m_b^2+\sqrt{\lambda}}{r^2(a-b)^2+m_a^2+m_b^2-\sqrt{\lambda}}\,. \end{aligned} \tag{7.27}$$

where we introduce the notation

$$\lambda(x,y,z)=x^2+y^2+z^2-2xy-2xz-2yz\,, \tag{7.28}$$

which enables us to define, for the purpose of our computation,

$$\lambda=\lambda(-r^2(a-b)^2,\alpha^2,\beta^2)=(\alpha^2-\beta^2)^2+2(\alpha^2+\beta^2)r^2(a-b)^2+r^4(a-b)^4\,. \tag{7.29}$$

For $J^c_{m_am_b}$ we get

$$\begin{aligned} J^c_{m_am_b} &= \frac{2\pi r^2(a-b)}{\sqrt{\lambda}}\left[\frac{1}{\sqrt{\lambda}+m_a^2-m_b^2+r^2(a^2-b^2)}\ln\frac{a(\sqrt{\lambda}+r^2(a-b)^2+m_a^2-m_b^2)}{b(\sqrt{\lambda}-r^2(a-b)^2+m_a^2-m_b^2)}\right. \\ &\left.+\frac{1}{\sqrt{\lambda}+m_b^2-m_a^2+r^2(b^2-a^2)}\ln\frac{a(\sqrt{\lambda}-r^2(a-b)^2-m_a^2+m_b^2)}{b(\sqrt{\lambda}+r^2(a-b)^2-m_a^2+m_b^2)}\right] \\ &-\frac{\pi}{a(b^2r^2+m_b^2)-b(a^2r^2+m_a^2)}\ln\frac{a(b^2r^2+m_b^2)}{b(a^2r^2+m_a^2)}\,. \end{aligned} \tag{7.30}$$

The $\ln\frac{a}{b}$ terms which apparently give divergencies when a or b goes to zero are spurious: indeed they cancel because of the symmetrical way the function $J^c_{m_am_b}$ appears in $a(\underline{r};Q_1,Q_2;z_1,z_2)$, $b(\underline{r};Q_1,Q_2;z_1,z_2)$ or $f(\underline{r};Q_1,Q_2;z_1,\,z_2)$.

Let us now consider the J_{3m} integral. After performing a special conformal transformation, namely an inversion on momentum integration variables and other dimensional vectors and parameters, a translation and again an inversion, we arrive to integrals with smaller number of propagators which are calculated in the standard way. The final result reads

$$\begin{aligned} J_{3m} &= \frac{2\pi}{r^2}\left\{\left(\frac{1}{r^2a^2+m^2}-\frac{1}{r^2\bar{a}^2+m^2}\right)\ln\frac{r^2a^2+m^2}{r^2\bar{a}^2+m^2}\right. \\ &\left.+\left(\frac{1}{r^2a^2+m^2}+\frac{1}{r^2\bar{a}^2+m^2}+\frac{2}{r^2a\bar{a}-m^2}\right)\ln\frac{(r^2a^2+m^2)(r^2\bar{a}^2+m^2)}{m^2r^2}\right\}\,. \end{aligned} \tag{7.31}$$

With the same but more tricky approach we can compute the J_{4mm} integral after performing a special conformal transformation; we refer to [7] for the complete calculation and final expression of this integral (see (A.66) and (A.67) of [7]). Starting from this result, we now derive another expression in such way that some spurious divergent terms (appearing when $r^2 = Q_i^2$, which corresponds to $a = 0$ or $b = 0$) explicitely cancel. Thus it allows us to use it in our numerical integration code (cf. sections 4 and 5). This makes the explicit expression (7.33) different from the one given in (A.67) of [7]. The resulting expression for $J_{4\mu_1\mu_2}$ is

$$
\begin{aligned}
&J_{4\mu_1\mu_2} = \qquad (7.32)\\
&\frac{1}{r^2(r^2\bar{z}_1^2+\mu_1^2)(r^2\bar{z}_2^2+\mu_2^2)} J_{3\alpha\beta}^{finite}\left(\frac{-z_1\bar{z}_1 r^2+\mu_1^2}{\bar{z}_1^2 r^2+\mu_1^2}, \frac{-z_2\bar{z}_2 r^2+\mu_2^2}{\bar{z}_2^2 r^2+\mu_2^2}, \frac{r^2\mu_1}{r^2\bar{z}_1^2+\mu_1^2}, \frac{r^2\mu_2}{r^2\bar{z}_2^2+\mu_2^2}, r\right)\\
&+\frac{1}{r^2(r^2 z_1^2+\mu_1^2)(r^2 z_2^2+\mu_2^2)} J_{3\alpha\beta}^{finite}\left(\frac{-z_1\bar{z}_1 r^2+\mu_1^2}{z_1^2 r^2+\mu_1^2}, \frac{-z_2\bar{z}_2 r^2+\mu_2^2}{z_2^2 r^2+\mu_2^2}, \frac{r^2\mu_1}{r^2 z_1^2+\mu_1^2}, \frac{r^2\mu_2}{r^2 z_2^2+\mu_2^2}, r\right)
\end{aligned}
$$

with

$$
\begin{aligned}
&J_{3\alpha\beta}^{finite}(a,\, b,\, \alpha,\, \beta,\, r) =\\
&\frac{\pi}{4}\Bigg\{\left(\frac{8}{a-b}+\frac{2\,(\alpha^2-\beta^2)}{(a-b)^2\,r^2}\right)\ln\frac{\alpha^2}{\beta^2}+\frac{4r^2\left(-4+r^2\left(\frac{a}{a^2\,r^2+\alpha^2}+\frac{b}{b^2\,r^2+\beta^2}\right)\right)\ln\frac{b^2\,r^2+\beta^2}{a^2\,r^2+\alpha^2}}{a\,(a-b)\,b\,r^2+b\,\alpha^2-a\,\beta^2}\\
&-2\,\ln\frac{\alpha^2\,\beta^2}{r^4}+\frac{2\,r^4}{(a^2\,r^2+\alpha^2)\,(b^2\,r^2+\beta^2)}\left(\ln\frac{\alpha^2\,\beta^2}{r^4}-2\,\ln\frac{\alpha^2\,\beta^2}{(a^2\,r^2+\alpha^2)\,(b^2\,r^2+\beta^2)}\right)\\
&-\frac{8}{(a-b)\,(a\,(a-b)\,b\,r^2+b\,\alpha^2-a\,\beta^2)\left(-a^2\,r^2+b^2\,r^2-\alpha^2+\beta^2+\sqrt{\lambda}\right)}\\
&\times\Bigg[\left(-(a-b)^2\,r^2-\alpha^2+\beta^2+\sqrt{\lambda}\right)\left(\frac{-a\,(b^2\,r^2+\beta^2)}{b}\,\ln\left(1+\frac{b^2\,r^2}{\beta^2}\right)\right. \qquad (7.33)\\
&\left.+\left(a^2\,r^2+\alpha^2\right)\,\ln\frac{a^2\,r^2+\alpha^2}{\beta^2}\right)+\left((a-b)^2\,r^2-\alpha^2+\beta^2+\sqrt{\lambda}\right)\\
&\times\left(\frac{-b\,(a^2\,r^2+\alpha^2)}{a}\ln\left(1+\frac{a^2\,r^2}{\alpha^2}\right)+\left(b^2\,r^2+\beta^2\right)\,\ln\frac{b^2\,r^2+\beta^2}{\alpha^2}\right)\Bigg]\\
&+\Bigg(\frac{\left(a^2\,r^2-b^2\,r^2+\alpha^2-\beta^2+\sqrt{\lambda}\right)^2}{(a-b)^2\,r^2\,\sqrt{\lambda}}+\frac{8\,(a-b)\,r^4\,\left(-4+r^2\,\left(\frac{a}{a^2\,r^2+\alpha^2}+\frac{b}{b^2\,r^2+\beta^2}\right)\right)}{\left((a^2-b^2)\,r^2+\alpha^2-\beta^2+\sqrt{\lambda}\right)\,\sqrt{\lambda}}\\
&+\frac{8\,\sqrt{\lambda}}{(a-b)\,(a\,(a-b)\,b\,r^2+b\,\alpha^2-a\,\beta^2)}\Bigg)\ln\frac{(a-b)^2\,r^2+\alpha^2-\beta^2+\sqrt{\lambda}}{-(a-b)^2\,r^2+\alpha^2-\beta^2+\sqrt{\lambda}}\\
&+\left(\frac{-\left(-a^2\,r^2+b^2\,r^2-\alpha^2+\beta^2+\sqrt{\lambda}\right)^2}{(a-b)^2\,r^2\,\sqrt{\lambda}}+\frac{8\,(a-b)\,r^4\,\left(-4+r^2\,\left(\frac{a}{a^2\,r^2+\alpha^2}+\frac{b}{b^2\,r^2+\beta^2}\right)\right)}{\left((-a^2+b^2)\,r^2-\alpha^2+\beta^2+\sqrt{\lambda}\right)\,\sqrt{\lambda}}\right)
\end{aligned}
$$

$$\times \ln \frac{-(a-b)^2 r^2 - \alpha^2 + \beta^2 + \sqrt{\lambda}}{(a-b)^2 r^2 - \alpha^2 + \beta^2 + \sqrt{\lambda}} + \left[\frac{16\, r^2}{\sqrt{\lambda}} + \frac{2\, r^2 \left(4 + r^2 \left(- \left(\frac{1}{a^2\, r^2 + \alpha^2} \right) - \frac{1}{b^2\, r^2 + \beta^2} \right) \right)}{\sqrt{\lambda}} \right.$$
$$\left. - 8 \frac{(a^2 - b^2)\, r^2 + \alpha^2 - \beta^2}{(a-b)\, \sqrt{\lambda}} - \frac{2\sqrt{\lambda}}{(a-b)^2 r^2} \right] \ln \frac{(a-b)^2 r^2 + \alpha^2 + \beta^2 + \sqrt{\lambda}}{(a-b)^2 r^2 + \alpha^2 + \beta^2 - \sqrt{\lambda}} \Bigg\} ,$$

where appropriate additional $\ln r^2$ terms have been introduced in order to write the final result as made of logarithms of dimensionless quantities. The difference between these two expressions only involves terms proportional to $\ln r^2$, in accordance to the dimensional regularization, since $J_{3\alpha\beta}$ is a divergent integral. However, at the level of the final result for $J_{4\mu_1\mu_2}$, which is both UV and IR finite, these additional terms of course cancel each other.

References

[1] E.A. Kuraev, L.N. Lipatov and V.S. Fadin, Phys. Lett. **B60** (1975) 50-52; Sov. Phys. JETP **44** (1976) 443-451; Sov. Phys. JETP **45** (1977) 199-204; Ya.Ya. Balitskii and L.N. Lipatov, Sov. J. Nucl. Phys. **28** (1978) 822-829.

[2] V. N. Gribov and L. N. Lipatov, Yad. Fiz. **15**, 781 (1972) [Sov. J. Nucl. Phys. **15**, 438 (1972)]; G. Altarelli and G. Parisi, Nucl. Phys. B **126**, 298 (1977); Y. L. Dokshitzer, Sov. Phys. JETP **46** (1977) 641 [Zh. Eksp. Teor. Fiz. **73** (1977) 1216].

[3] J. Bartels, A. De Roeck and H. Lotter, Phys. Lett. B **389**, 742 (1996); S. J. Brodsky, F. Hautmann and D. E. Soper, Phys. Rev. Lett. **78**, 803 (1997) [Erratum-ibid. **79**, 3544 (1997)]; J. Kwiecinski and L. Motyka, Phys. Lett. B **462**, 203 (1999); J. Bartels, C. Ewerz and R. Staritzbichler, Phys. Lett. B **492** (2000) 56; J. Kwiecinski and L. Motyka, Eur. Phys. J. C **18**, 343 (2000);V. P. Goncalves, M. V. T. Machado and W. K. Sauter, hep-ph/0611171.

[4] M. Boonekamp, A. De Roeck, C. Royon and S. Wallon, Nucl. Phys. B **555**, 540 (1999).

[5] J. Kwiecinski and L. Motyka, Phys. Lett. B **438**, 203 (1998).

[6] B. Pire, L. Szymanowski and S. Wallon, International Conference on Linear Colliders (LCWS 04), Paris, France, 19-24 Apr 2004, Published in "Paris 2004, Linear colliders, vol. 1," 335-340; 10th International Conference on Structure of Baryons (Baryons 2004), Palaiseau, France, 25-29 Oct 2004, Nucl. Phys. **A755** (2005) 626-629; 11th International Conference on Elastic and Diffractive Scattering, Blois, France, 15-20 May 2005, "Towards High Energy Frontiers", eds. M. Haguenauer et al., 373-376.

[7] B. Pire, L. Szymanowski and S. Wallon, Eur. Phys. J. C **44**, 545 (2005).

[8] R. Enberg, B. Pire, L. Szymanowski and S. Wallon, Eur. Phys. J. C **45** (2006) 759; "PHOTON 2005," Warsaw, 30 Aug - 8 Sep 2005, Acta Phys. Polon. B **37** (2006) 847.

[9] B. Pire, M. Segond, L. Szymanowski and S. Wallon, Phys.Lett.B639 (2006) 642-651.

[10] L. Mankiewicz and G. Piller, Phys. Rev. D **61**, 074013 (2000); D. Y. Ivanov and R. Kirschner, Phys. Rev. D **58** (1998) 114026; D. Y. Ivanov, R. Kirschner, A. Schafer and L. Szymanowski, Phys. Lett. B **478** (2000) 101 [Erratum-ibid. B **498** (2001) 295]; A. Ivanov and R. Kirschner, Eur. Phys. J. C **29** (2003) 353.

[11] A. D. Martin, M. G. Ryskin and T. Teubner, Phys. Rev. D **55** (1997) 4329; Phys. Rev. D **56** (1997) 3007; Phys. Rev. D **62** (2000) 014022.

[12] D. Y. Ivanov and A. Papa, Nucl. Phys. B **732** (2006) 183; hep-ph/0610042.

[13] V. M. Budnev, I. F. Ginzburg, G. V. Meledin and V. G. Serbo, Phys. Rept. **15** (1974) 181.

[14] I. F. Ginzburg, S. L. Panfil and V. G. Serbo, Nucl. Phys. B **284** (1987) 685.

[15] D. Y. Ivanov, M. I. Kotsky and A. Papa, Eur. Phys. J. C **38** (2004) 195.

[16] P. Ball, V. M. Braun, Y. Koike and K. Tanaka, Nucl. Phys. B **529** (1998) 323.

[17] V. M. Braun, G. P. Korchemsky and D. Mueller, Prog. Part. Nucl. Phys. **51** (2003) 311.

[18] S. Bethke, J. Phys. G **26** (2000) R27.

[19] ILC, Basic Conceptual Design Report, http://www.linearcollider.org.

[20] LDC outline document, http://www.ilcldc.org.

[21] M. Davier, M. E. Peskin and A. Snyder, hep-ph/0606155.

[22] G. T. Bodwin, E. Braaten, J. Lee and C. Yu, Phys. Rev. D **74**, 074014 (2006).

[23] L. Lewin, *Polylogarithms and Associated Functions*, New York: North-Holland, 1981.

[24] B. Clerbaux and M. V. Polyakov, Nucl. Phys. A **679** (2000) 185.

[25] A. P. Bakulev and S. V. Mikhailov, Phys. Lett. B **436** (1998) 351.

[26] V. P. Goncalves and W. K. Sauter, Eur. Phys. J. C **44** (2005) 515; Phys. Rev. D **73** (2006) 077502.

[27] S. Braunewell and C. Ewerz, Phys. Rev. D **70** (2004) 014021.

[28] A.N. Vasil'ev, *The Field Theoretic Renormalization Group in Critical Behavior theory and Stochastic Dynamics*, Chapman and Hall/CRC.